To: chris.barker@noaa.gov[chris.barker@noaa.gov]; CJ.Beegle-Krause@sintef.no[CJ.Beegle-Krause@sintef.no]; Conmy, Robyn[Conmy.Robyn@epa.gov]; Thomas.s.coolbaugh@exxonmobil.com[Thomas.s.coolbaugh@exxonmobil.com]; fingasmerv@shaw.ca[fingasmerv@shaw.ca]; ali.khelifa@ec.gc.ca[ali.khelifa@ec.gc.ca]; jrpayne@sbcglobal.net[jrpayne@sbcglobal.net]; wspegau@pwssc.org[wspegau@pwssc.org]; creddy@whoi.edu[creddy@whoi.edu]
Cc: nancy.kinner@unh.edu[nancy.kinner@unh.edu]
From: Mandsager, Kathy
Sent: Wed 5/18/2016 7:18:18 PM
Subject: state-of-science: transport and behavior group
1-s2.0-S0278434313000782-main.pdf
2016.05.17_INPUT REVISIONS with NEK clean-up at 6 PM_CRRC state-of-science on Physical Transport and Chemical Behavior for public input.docx
references from public input.docx

Thanks for making headway on incorporating the public input into your document. Attached is the draft after yesterday's session. I'm also attaching the Weingartner et al 2013 reference for your perusal. The references that were suggested via the public input process will eventually be incorporated into the database. But please let me know if you are unable to access a particular manuscript for review.

In order to schedule a couple more meetings, please fill in all 2-hour time slots on the doodle poll that you can possibly attend. This has been tine-zone enabled for you convenience and if you could make your selection by early next week that would be helpful in order to secure these dates over our busy summer months. Thank you!

Doodle poll Here>> http://doodle.com/poll/iu423v2aywfkcyfx

Kathy Mandsager

Coastal Response Research Center

Center for Spills and Environmental Hazards

220 Gregg Hall, 35 Colovos Rd

University of New Hampshire

Durham, NH 03824

603.862.1545

Continental Shelf Research 67 (2013) 5–22

Contents lists available at ScienceDirect

Continental Shelf Research

journal homepage: www.elsevier.com/locate/csr

Research papers

Hydrographic variability over the northeastern Chukchi Sea shelf in summer-fall 2008–2010

Thomas Weingartner [n], Elizabeth Dobbins, Seth Danielson, Peter Winsor, Rachel Potter, Hank Statscewich

University of Alaska, School of Fisheries and Ocean Science, Fairbanks, AK 99775, United States

article info

Article history:
Received 22 May 2012
Received in revised form
14 February 2013
Accepted 19 March 2013
Available online 28 March 2013

Keywords:
Chukchi Sea
Stratification
Circulation
Water properties
Seasonal and interannual variations

abstract

We used shipboard CTD, mooring, meteorological, glider, and high-frequency radar data to examine spatial and temporal (seasonal and interannual) variations in the circulation and water properties over the central portion of the northeastern Chukchi Sea shelf from August–October of 2008, 2009, and 2010. Seasonally, warm and moderately saline Bering Sea Water (BSW) replaces cool, dilute surface meltwaters and cold, saline, sub-surface, winter-formed waters. BSW advection thus affects shelf stratification and the heat budget with oceanic heat flux convergence supplanting solar heating as the dominant shelf heat source by September. BSW spreads eastward from the Chukchi's Central Channel, so that water property and stratification transitions proceed from west to east across the study region. Models predict a mean clockwise flow around Hanna Shoal (which lies to the north of the study area) suggesting winter-formed waters from northeast of the Shoal are advected southwestward into a portion of the study area. The observations, though limited, support this notion. We hypothesize that the convergence of BSW from the west and winter waters from the northeast leads, in some years, to large horizontal variations in water properties, stratification, and ocean heat flux convergence over spatial scales of 50–100 km.

Interannual variations in summer/fall shelf water properties appear linked to processes occurring in the Bering and/or southern Chukchi Sea, and the regional winds (which affect the local circulation). Although there were large interannual differences in shelf-wide ice retreat patterns from May–July, these differences were not reflected in late summer water properties.

1. Introduction

Seasonal changes in Chukchi Sea water properties are established by the annual cycles of sea–ice formation and ablation, heating and wind mixing, and transport of waters from Bering Strait. In summer and early fall, the Strait transport is northward on average and includes three major water masses, which following the nomenclature of Coachman et al. (1975) and Walsh et al. (1989) are: cold, salty, nutrient-rich Anadyr Water; warm, fresh, nutrient-poor Alaskan Coastal Water (ACW); and Bering Shelf Water. The latter has properties intermediate between, but nonetheless distinct from, the Anadyr and Alaskan Coastal water masses. Coachman et al. (1975) maintain that the Anadyr and Bering Shelf water masses mix to form Bering Sea Water (BSW) north of the Strait, whereas ACW maintains its properties on the Chukchi shelf. In summer and fall, Chukchi bottom waters often include near-freezing, saline (dense) waters that formed in the previous winter during freezing over both the Bering and Chukchi seas. In addition, shallow plumes of cool, dilute, surface waters, formed by ice melt, may also be present.

BSW is transported to the northwest Chukchi, over the central shelf, and northward through the Central Channel (Fig. 1a; Weingartner et al., 2005; Woodgate et al., 2005a, 2005b). Weingartner et al. (2005) suggested that, south of Hanna Shoal, some central-shelf waters flow eastward toward the coast, in agreement with the circulation models of Winsor and Chapman (2004) and Spall (2007). North of the Central Channel, where there are no long-term current measurements, both models suggest the average flow follows the bathymetry around the western and northern flanks of Hanna Shoal. From here, the flow moves southward along the eastern side of the Shoal (presumably between the 40 m and 60 m isobaths) before eventually entering Barrow Canyon. However, the models also predict that some of the water along the east side of Hanna Shoal penetrates southwestward along the southern edge of the Shoal before turning eastward towards the coast. The ACW flows northeastward within the Alaskan coastal current toward the head of Barrow Canyon. Here it merges with waters flowing eastward from the central shelf to form the canyon outflow. Hence in summer and fall, the canyon outflow contains a horizontally- and vertically-structured complex of water masses (Pickart et al., 2005; Shroyer and Plueddemann, 2012) that

[n] Corresponding author. Tel.: +1 907 474 7993.
E-mail address: jweingartner@alaska.edu (T. Weingartner).

0278-4343
http://dx.doi.org/10.1016/j.csr.2013.03.012

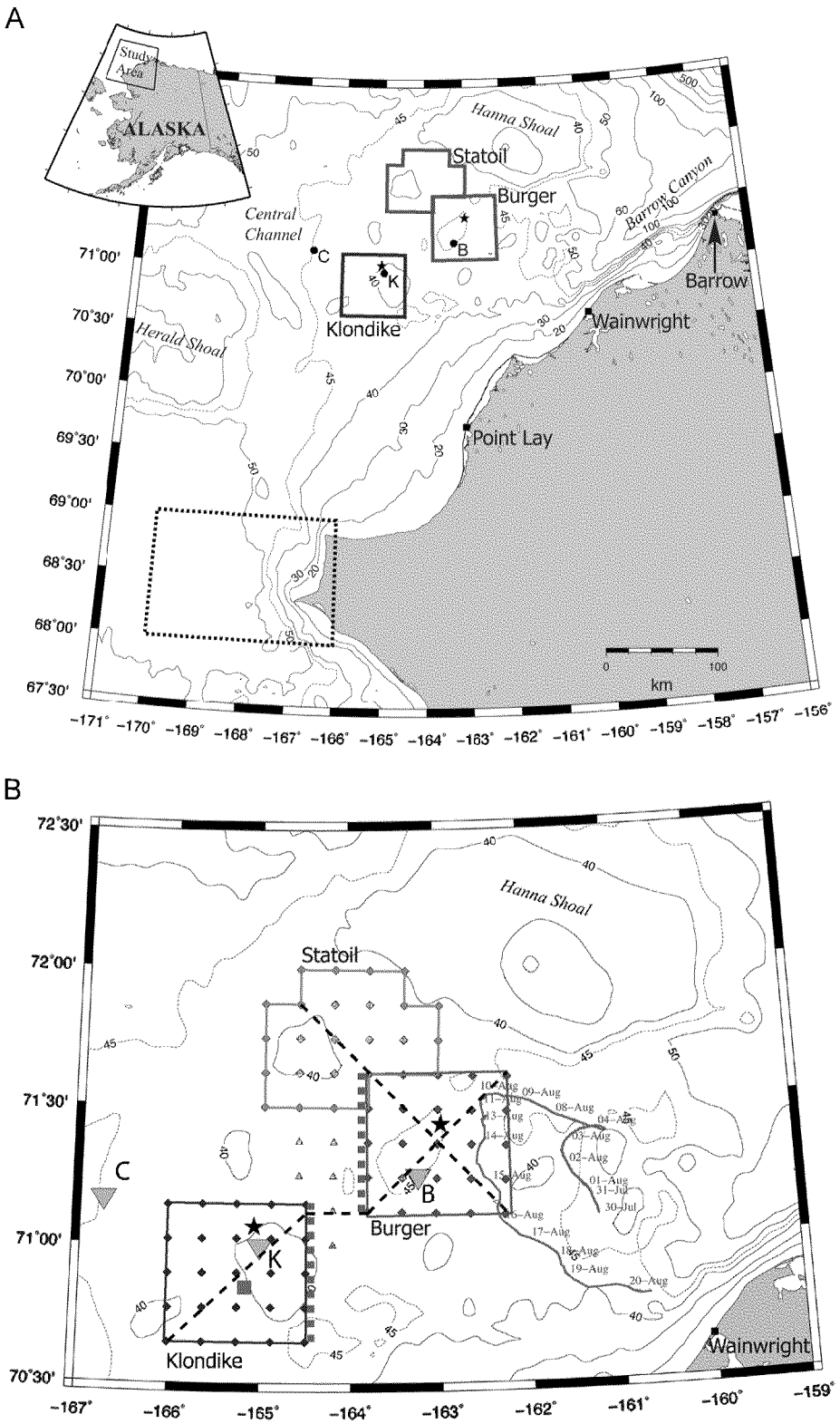

Fig. 1. (a) Map of the eastern Chukchi Sea showing bathymetry and place names. CTD surveys were conducted in Klondike and Burger (2008–2010) and Statoil (2010 only). The 2009 mooring locations at Crackerjack, Klondike, and Burger, are denoted by C, K, and B, respectively. Stars indicate the locations of the NARR gridpoints used in the heat budget analyses. The box outlined by the dotted line and centered at 68130′N and 1681W, denotes the area used to estimate sea surface temperatures from satellite thermal imagery. (b) Detailed map of the study region showing the nominal distribution of CTD stations in 2008–2010 Klondike (blue diamonds), Burger (red diamonds) and, in 2010 only, Statoil (green diamonds) and additional stations (orange triangles). The boxes delineating each of these areas served as the control volumes in the heat budget estimates. The Crackerjack (C), Klondike (K) and Burger (B) moorings are indicated by cyan inverted triangles, the Klondike met buoy by a green square and the NARR grid points by black stars. The blue line to the east and south of Burger is the 2010 glider transect with dates indicating the daily position of the glider. The stations intersected by the diagonal dashed lines across Klondike and Burger were used in constructing the sections shown in Fig. 4 in 2009 and 2010. The stations forming the eastern boundary of Klondike and the western boundary of Burger (indicated by the green dotted line) were used to construct the sections shown in Fig. 4 for 2008. The stations along the dashed line running diagonally across Burger and Statoil were used in constructing the sections of Fig. 8 in 2010. (For interpretation of the references to color in this figure legend, the reader is referred to the web version of this article.)

include ACW, meltwater, dense winter waters, BSW, and mixtures of each.

To a large extent the Chukchi circulation appears consistent with barotropic, geostrophic dynamics in which the shelf pressure field arises as a response to wind-forced convergences and divergences and to the mean pressure difference between the Pacific and Arctic oceans. The latter provides the impetus for the northward transport through Bering Strait. Even though much of the Chukchi shelf has a gently varying bathymetry, topographic control appears to exert an important influence on the shelf dynamics. Thus, north of the Strait the model streamlines parallel contours of f=h (where f is the Coriolis parameter and h is the water depth). Over the northeastern shelf, mean winds are from the east-northeast so that in the mean, the flow opposes the winds. Nevertheless, flow variations are primarily wind-forced and occasionally the wind stress can be sufficiently strong to reverse the flow (Weingartner et al., 1998, 2005).

The measurements reported herein were collected to provide the physical context for the biological studies that were simultaneously conducted and reported upon in this volume. The area of interest is southwest of Hanna Shoal and east of the Central Channel (Fig. 1a) and lies more than 150 km offshore. This distance exceeds the barotropic radius of deformation (140 km for a 40 m deep shelf), so the survey areas are likely not within the direct influence of the Alaskan coastal current, and the effects of wind-forced coastal convergences/divergences are expected to be somewhat reduced. We describe the seasonal, interannual, and regional differences in water properties and offer insights on some of the processes controlling the observed spatial and temporal differences in this portion of the Chukchi Sea.

The paper is organized as follows. In the next section, we describe the various data sets used and their processing. Section 3 presents the results, beginning with a description of the seasonal retreat of ice across the shelf (Section 3.1). Section 3.2 describes results from the CTD surveys with an emphasis on seasonal, interannual, and spatial variations in temperature and salinity across the study areas. These reveal considerable spatial complexity, which is not obviously linked to patterns of ice retreat. Instead, the property characteristics appear largely attributable to differential patterns of oceanic advection, as inferred from an analysis of the heat budget (Section 3.3), and supplemented by observations from gliders and coastal high-frequency radar measurements of the regional surface circulation. Section 3.4 describes a limited set of moored current measurements that provide further insights on circulation patterns and dynamics. The results of this section complement, to some extent, the inferences of Section 3.3. Section 4 integrates the results and places them in a broader context, while Section 5 concludes the paper.

2. Methods

2.1. CTD surveys

In 2008 and 2009, we conducted three cruises in the Klondike and Burger study areas (Fig. 1a). In 2010, a third study area, Statoil, was added; Klondike and Statoil were sampled twice and Burger sampled three times. In general, cruises occurred in late July/early August, late August/September, and late September to early October, although the timing of each cruise varied among years (Table 1). Klondike and Burger are 55-km └ 55-km squares containing 25 stations each (Fig. 1b), Statoil has the same area, but is shaped differently. In 2010, additional stations were sampled to improve spatial continuity among the various study areas.

Bottom depths in the study areas are 40–45 m. Klondike and Statoil are east of the Central Channel, a 45–50 m deep depression

Table 1
Cruise dates and nomenclature.

Identifier	Klondike		Burger	
	Sampling dates	Median date	Sampling dates	Median date
JA08	Jul. 24–Aug. 1	Jul. 27	Aug. 2–10	Aug. 4
AS08	Aug. 21–Sep. 1	Aug. 27	Sep. 4–22	Sep. 16
SO08	Sep 24–28	Sep. 26	Oct. 2–12	Oct. 7
A09	Aug. 10–24	Aug 27	Aug. 17–27	Aug.22
S09	Sep. 3–11	Sep. 8	Sep. 13–17	Sep. 15
SO09	Sep. 25–29	Sep. 27	Oct. 2–10	Oct. 6
A10	Aug. 8–16	Aug. 12	Aug. 16–22	Aug. 19
AS10	Aug 31–Sep. 7	Sep 3	Sep. 8–14	Sep. 11
O10	–	–	Oct. 1–5	Oct. 3

running northward between about 1671W and 1701W (Fig. 1a and b). Statoil and Burger lie to the south of Hanna Shoal, an east-west elongated bank with minimum depths of o 25 m. On the southeast side of the Shoal, the isobaths diverge; the 50 m isobath extends southward, but the 40 and 45 m isobaths trend southwestward. Between 691N and 70.51N (south of Klondike) the isobaths trend to the northeast before veering eastward toward the coast along 70.51N (Fig. 1a).

During the first cruise in 2008, data from several casts in southwestern Klondike were inadvertently lost, and several of the planned stations in the northeastern corner of Burger could not be occupied due to ice. CTD data were collected using a Seabird, Inc. SBE-19+V2 CTD sampling at 4 Hz and lowered through the water column at 10 m min^{-1}. The instrument measured pressure, temperature, conductivity, and fluorescence. Data were processed followed the manufacturer's procedures and were then averaged into 1 dbar bins. Comparison of pre- and post-season calibrations (performed by Seabird) of the temperature and conductivity sensors indicate that the data are accurate to better than 0.005 1C for temperature and 0.02 for salinity.

2.2. Meteorological and sea–ice concentration data

We constructed daily ice concentration maps for the May 1–July 30 period of each year using the Advanced Microwave Scanning Radiometer—Earth Observing System (AMSRE-E) data sets prepared by Universitat Bremen following Spreen et al. (2008). A subset of these are shown to illustrate the seasonal progression of ice retreat in each year prior to the surveys (Fig. 2). We obtained 3-h estimates of the winds for the region from the National Center for Environmental Prediction North American Regional Re-analysis (NARR) model hindcasts (Mesinger and Coauthors, 2006). The gridpoints used are shown in Fig. 1a and listed in Table 2.

Approximate heat budgets were estimated over control volumes between successive cruises to assess the differences in advective tendencies among the study sites. The heat budgets were calculated accordingly:

$$Q_w - \underbrace{\delta(1-\alpha)Q_{solar} + Q_{longwave} + \delta Q_{latent} + Q_{sensible}}_{Q_{as}} + \sum Q_{oc}$$

The first term on the left (Q_w) is the rate of change through time of heat in the water column. Q_w was computed as the difference in heat between successive surveys within each control volume (defined by the boundaries of each study site) divided by the time interval based on the median cruise dates in each area. The term in brackets represents the net heat flux between the ocean and atmosphere (Q_{as}). This term includes the albedo-corrected ($1-\alpha$; $\alpha = 0.07$) net incoming solar radiation (Q_{solar}), measured by the Department of Energy's Atmospheric Radiation Measurement

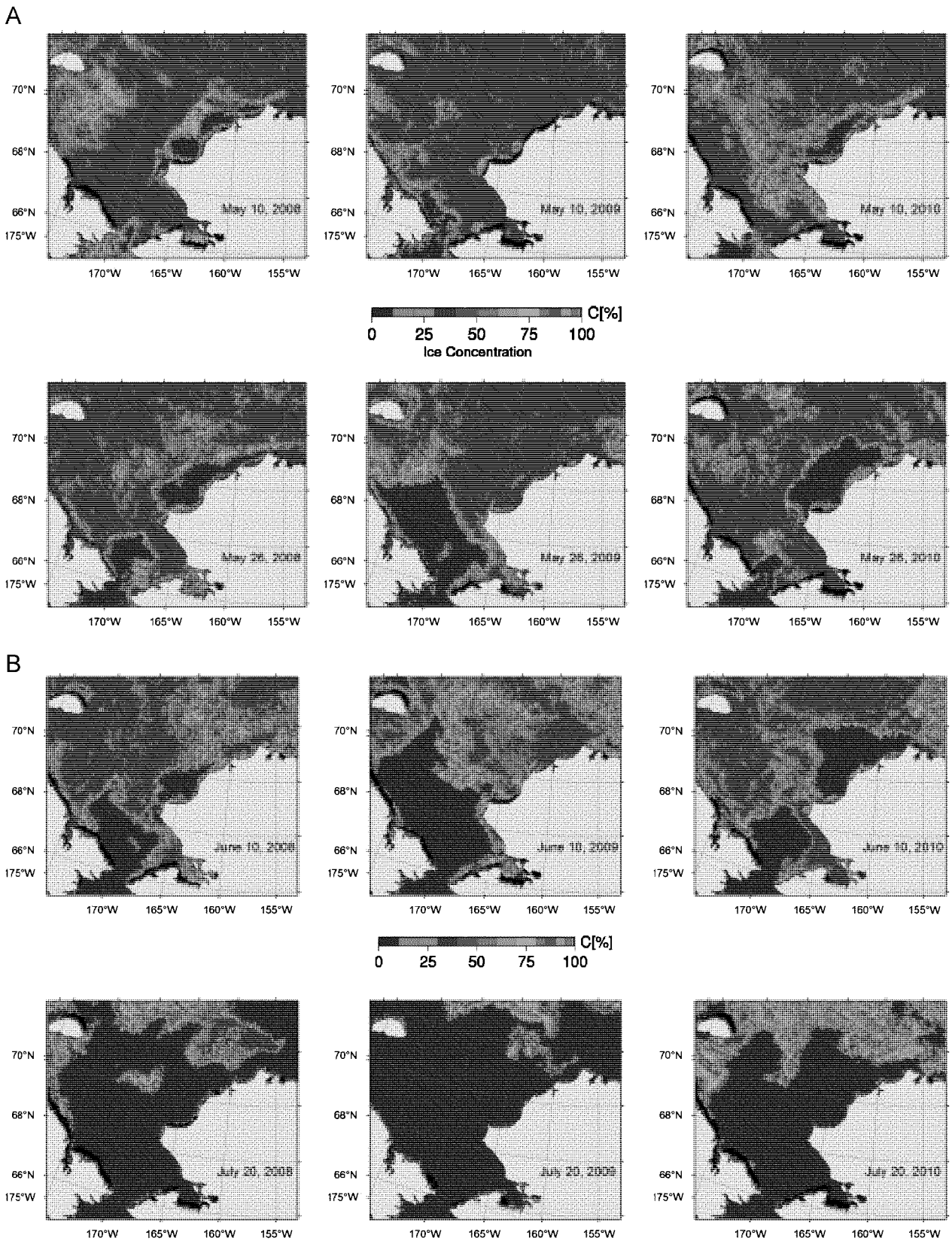

Fig. 2. (a) Mean daily sea–ice concentration maps for the Chukchi Sea based on AMSR-E satellite imagery. The years are 2008 (left column), 2009, (middle column), and 2010 (right column) and the dates are May 10 (1st row) and May 26 (2nd row). (b) Mean daily sea–ice concentration maps for the Chukchi Sea based on AMSR-E satellite imagery. The years are 2008 (left column), 2009, (middle column), and 2010 (right column) and the dates are June 10 (1st row) and July 20 (2nd row).

(ARM) Climate Research Facility in Barrow, Alaska. (ARM data were collected once per minute, which we then averaged into daily means.) ARM data were used rather than the NARR estimates of Q_{solar} to avoid possible errors associated with model limitations pertaining to clouds (Ladd and Bond, 2002; Walsh et al., 2009). The largest single source of error in Q_{solar} is associated with the

Table 2
Position information for the current meter moorings, meteorological buoy, and principal NARR gridpoints used in the analyses.

Mooring	Latitude (N)	Longitude (W)	Bottom depth (m)	Data depths (m)
Klondike	70159.93′	16510.051′	45	7, 23, 35
Burger	71114.39′	163116.81′	45	7, 23, 35
Crackerjack	71110.18′	166144.93′	46	8, 20, 36
Klondike MetBuoy	70152.38′	165114.90′	40	1
Klondike NARR	7113.75′	16513.75′		
Burger NARR	71126.25′	16310.0′		

assumption that the Barrow measurements represent those in the survey area. Although cloud-cover variations between Barrow and the survey area could cause large day-to-day variations in Q_{solar}, these differences should be negligible when averaged over many days as done here. This assumption is supported by inspection of satellite imagery of the northeast Chukchi Sea obtained from NOAA polar orbiting satellites. We examined 12 satellite images per day and concluded that cloud cover differences between Barrow and the study sites were small when considered over several days or longer. The third term is the net longwave radiation ($Q_{longwave}$) based on the NARR model. These may also suffer from cloud-bias in the NARR model (Walsh et al., 2009). We compared averages of these values to those computed following Josey et al. (2003) for the same time period. Their method requires cloud cover, air, dewpoint, and sea surface temperatures (SST) data. For SST, we used the average surface temperature in each survey area derived from the CTD data. Mean monthly cloud cover values are from the climatology of Brower et al. (1988) and the mean air temperature and relative humidity (from which dewpoint was calculated following Lawrence (2005)) were measured at the National Weather Service station in Barrow. The fourth term consists of the latent and sensible heat fluxes ($Q_{latent}+Q_{sensible}$) obtained from the NARR 3-h forecast values in each study region. The residual that remains after estimating the terms on the left-hand side of the equation is ascribed to be the net oceanic heat flux convergence, Q_{oc}, which includes both horizontal advection and lateral mixing.

It is difficult to assign rigorous uncertainty estimates to the heat budget terms. Berry and Kent (2009) indicated uncertainties of 10 W m^{-2} in NCEP estimates of Q_{latent} and $Q_{sensible}$ in comparison with high-quality buoy measurements made at 601N, 211W in the North Atlantic Ocean. Josey et al. (2003) estimate that the random error in $Q_{longwave}$ is 2 W m^{-2} when compared with direct observations. The largest uncertainty in our estimate of $Q_{longwave}$ pertains to using a climatological value for the cloud cover fraction (0.9 in August and September); a difference in the cloud cover fraction of 7 0.1 leads to □20 W m^{-2} difference in $Q_{longwave}$. Upon comparing NARR $Q_{longwave}$ with those based on Josey et al.'s method we find the rms difference to be 25 W m^{-2}. Considering the errors in $Q_{longwave}$, Q_{latent}, and $Q_{sensible}$, Q_{ocean} is deemed undetermined if $|Q_w|$ o 30 W m^{-2}. The mean, standard errors, and 95% confidence limits on Q_{as} and vertically-averaged temperatures were estimated by standard bootstrapping (Manly, 1997), in which we resampled (with replacement) the data set from each time interval. Although stable values of the resulting statistical estimates were reached after 250 trials, all succeeding calculations were based on a sample size of 2000. We also compared standard bootstrapping with other bias-corrected and/or accelerated methods (Manly, 1997) and found that all methods yielded statistically identical results. The standard error on Q_w was then estimated by propagation of the bootstrapped standard error for the vertically-averaged temperatures. The resulting standard error was multiplied by 1.96 to form approximate 95% confidence limits on Q_w. Confidence limits on Q_{oc} were formed similarly based on the standard errors for Q_{as} and Q_w.

2.3. Mooring data

For 2009, we examined data from 307 kHz ADCPs (sampling every 30-min and in 4-m depth bins) and thermistors from moorings in the Central Channel (Crackerjack mooring site) and within Klondike and Burger (Table 2). Instruments were moored 2 m above the seabed. Data processing procedures are given by Mudge et al. (2010). Although some of the moorings recorded year-round or nearly so, our interest here is solely on the August through early October periods; when the shipboard surveys were conducted. The velocity data were low-pass filtered with a 35-h cutoff period prior to analysis. Confidence limits were based on the effective number of degrees of freedom using an integral time scale of 2 days computed following Emery and Thomson (2001). This time scale was derived from the autocovariance functions of the current and wind data for July through early October. This restricted interval ensured a large enough sample size for reliably estimating the integral time scale, and excluded periods of ice cover and/or strong fall storm winds in the analysis. In 2010, a meteorological buoy was deployed in Klondike (Table 2) from August through mid-September. The buoy measured wind velocity, sea surface temperatures, and currents at 1 m below the hull from a Nortek Aquadopp acoustic current meter. Current velocities were sampled at 1 Hz, averaged over 60 s, and recorded every 15-min.

2.4. High-frequency radar data

During the 2009 and 2010 open water season, we measured surface currents in the northeastern Chukchi Sea within 160 km of the coast at 6 km resolution using shore-based high-frequency radar (HFR) systems (manufactured by CODAR Ocean Sensors) located in Barrow, Wainwright, and Point Lay (Fig. 1a). Data collection from the Wainwright and Barrow sites began in September 2009 (mid-July 2010) and ended in mid-November of both years. The Pt. Lay site became operational in mid-September 2010 and ended in mid-November. The HFR measures currents within the upper 2 m of the water column based on the theory and operational procedures of Barrick et al. (1985). Antennae were calibrated by using a beam pattern measurement to correct for background noise in the frequency spectrum (Barrick and Lipa, 1986, Kohut and Glenn, 2003). Spatial and temporal coverage varies depending upon sea state and ionospheric interference (Teague, 2001). The latter, which reduces the signal-to-noise ratio, was maximal at night and minimal during the day. Capes to the north of Wainwright and Pt. Lay interfere with signal propagation and result in spatial gaps in the coverage. Data were acquired hourly and processed using the measured radar calibration pattern. For each hourly data set, we removed grid cells having less than 50% data return or velocities 4 3 m s^{-1}. (The latter choice is based on previous data sets within the HFR mask, including Barrow Canyon. Over the canyon moored ADCPs and HFR data indicate that maximum currents are 2.5 m s^{-1}. At distances greater than 30 km from the canyon axis maximum currents are o 1 m s^{-1}.) At each of the remaining gridpoints, we removed velocity components that exceeded three standard deviations.

2.5. Autonomous underwater vehicle (AUV) glider data

High-resolution hydrographic data was sampled during the open water season of 2010 using CTD data collected by a Teledyne-Webb Slocum glider equipped with a Seabird Glider Payload pumped CTD (GPCTD). The GPCTD data (pressure, temperature,

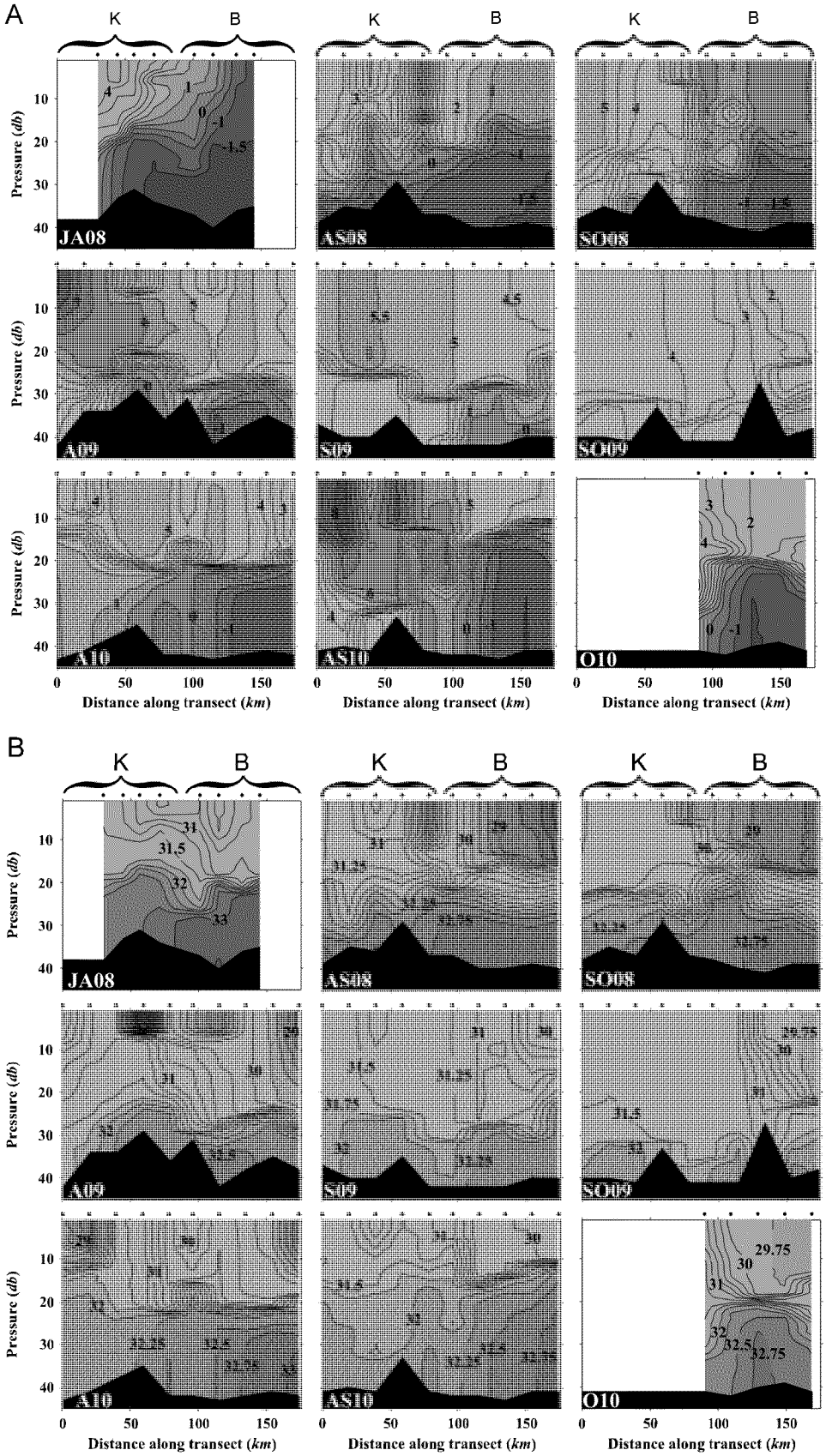

Fig. 3. (a) Temperature sections across Klondike (K) and Burger (B) in 2008 (upper row), 2009 (middle row), and 2010 (bottom row). Contour interval ¼0.5 1C. Cruise abbreviations are described in Table 1 and the location of the sections are shown in Fig. 1b. Dots at the top of each figure indicate station locations. Depths reflect cast depth. Each row represents a year. Columns are ordered with the first occupation of the section in any year in the first column and the last occupation for the year in the third column. (b) Salinity sections across Klondike (K) and Burger (B) in 2008 (upper row), 2009 (middle row), and 2010 (bottom row). Cruise abbreviations are described in Table 1 and the location of the sections are shown in Fig. 1b. Dots at the top of each figure indicate station locations. Depths reflect cast depth. Each row represents a year. Columns are ordered with the first occupation of the section in any year in the first column and the last occupation for the year in the third column.

conductivity) were processed following the manufacturer's recommendations and screened for spikes, corrupt data, and density inversions. After editing, the data were averaged into 1-dbar bins. The gliders typically flew with a 26 1 pitch angle to the vertical, and at an average vertical speed of 15 cm s^{-1} and a horizontal speed of 35 cm s^{-1}. The glider CTD sampling was at 0.5 Hz, which allowed a vertical resolution of 1 dbar. The glider undulates through the water column as it moves horizontally from one waypoint to the next. For the relatively shallow depths of the Chukchi Shelf the glider paths yielded a horizontal resolution of 200 m between the crest of vertical yo–yo pairs.

3. Results

3.1. Ice retreat patterns 2008–2010

A subset of daily AMSR-E sea–ice concentration maps (Fig. 2) shows considerable differences in seasonal patterns of ice retreat over the Chukchi shelf. Ice covered the entire shelf, including Bering Strait, at the beginning of May of each year (not shown), after which rapid changes in ice concentrations developed.

For example, by 10 May 2008, ice concentrations in and to the north of Bering Strait were high but lower south of the Strait (not shown), while open water developed over the northeastern shelf within a 100 km wide band along the Alaskan coast between about 681N and 71.31N. This opening followed the onset of 7 m s^{-1} northeasterly winds, which abated by mid-May. By 26 May, ice retreat progressed northward from Bering Strait into the southern Chukchi shelf, while the open water area over the northeastern shelf expanded slightly. Ice retreat continued over the southern Chukchi Sea through 10 June, but concentrations increased again farther offshore of the northwest coast of Alaska.

Ice retreat in early May 2010 was similar to that of 2008 in that a 100 km wide band of open water developed along the Alaskan coast over the northeastern shelf in response to moderate winds from the northeast. This band continued to widen offshore because winds generally remained moderately strong from the east-northeast. Hence, by mid-June, most of the northeastern shelf was ice-free.

In contrast to 2008 and 2010, winds in May 2009 were more southerly on average. Heavy ice covered the northwestern coast of Alaska, although retreat had begun in Bering Strait and along the Siberian coast. Ice retreat accelerated through May 2009 in the southern and western Chukchi, but the northeastern shelf remained heavily ice covered until mid-June. At that time moderate northeasterly winds developed, and ice began retreating from the northwestern coast of Alaska.

By late June of each year, the southern shelf was nearly ice-free, although there were considerable interannual differences in ice cover over the northern shelf. Through July, ice retreat progressed predominantly from south to north so that by 20 July, the entire shelf was ice free, except for moderately heavy ice concentrations over Herald Shoal (701N, 1701W) in 2008 and 2010, and Hanna Shoal (721N, 1621W) in all years. Martin and Drucker (1997) suggest that Taylor columns form over both shoals, impeding ice displacement and the intrusion of warmer Bering Sea summer waters onto the shoals. Once the ice has melted, the shoals serve as a potential reservoir for meltwaters (Weingartner et al., 2005). Synthetic aperture radar (SAR) imagery (not shown) for late July shows ice coverage of 30–50% over Hanna Shoal in all years (and over Herald Shoal in 2008 and 2010). August SAR imagery indicated that Hanna Shoal was ice-free in 2009 and 2010, but ice-covered through much of August 2008.

3.2. Temperature/salinity distributions

In this section we describe briefly, the spatial, seasonal, and interannual variations in temperature and salinity in each study area using a combination of section plots and plan views. We first consider the temperature and salinity sections (given on the map in Fig. 1a) shown in Fig. 3a and b. (Comparable density sections are shown in Fig. 11 of Gall et al., 2013) The section nomenclature follows Table 1; AS09 implies that the data along this transect were collected on the August–September cruise in 2009.

In 2008, the JA08 sections show that waters within 10–20 m of the bottom consisted of cold (≤−1 1C) and salty (≥32.5) dense waters formed over the previous winter. Warmer (≥0 1C) and fresher (≤31) waters enveloped the upper half of the water column of Burger (and in some portions of Klondike not included in the figure). Over the remainder of Klondike upper layer waters were warmer (2–4 1C) and moderately saline (31.5 o S o 32.5). Klondike waters warmed and freshened throughout 2008. Below 20 m, these changes reflect the replacement of winter waters by BSW. Within the upper layer of Klondike, some dilution occurred due to infiltration of low-salinity (≤31) waters; most likely meltwater filaments that were advected into the area and warmed by solar heating. Within Burger the bottom waters remained cold and salty and meltwaters occupied the upper 15 m throughout 2008.

Conditions in 2009 were very different from those in 2008 in several ways. During A09, the uppermost 15 m included shallow low-salinity (o 30) plumes with temperatures generally o 5 1C. Below the plumes and to 25 m depth (and elsewhere at the surface), warmer (5–6 1C) and saltier (31–31.5) waters were present. Bottom water temperatures and salinities were also substantially warmer and less saline in 2009; temperatures ranged from −1 t o 21C and salinities varied from 32 to o 32.5, with the densest bottom waters in the northeastern half of Burger. By the S09 survey, the low-salinity surface plumes were absent from Klondike, and the upper 30 m had nearly vertically-uniform temperatures (5–6 1C) and salinities (31–31.5). Bottom waters had warmed also and were generally 4 2 1C. However, Burger bottom waters still consisted of cold, salty, winter water. By the time of the SO09 survey, upper ocean temperatures had cooled to 3–4 1C across the section. There was little change in salinity except in the northeast corner of Burger where low salinity (≤30) waters protruded to the southwest.

In August 2010 (A10), the upper 20 m included moderately warm (3–4 1C), low-salinity (o 30), meltwater pools interspersed within an otherwise homogeneous layer of warmer (5–6 1C), saltier (30–31.5) water. The lower half of the water column contained cold (o 1.5 1C), salty (4 32) waters, with the coldest and saltiest waters in Burger. By the AS10 survey much of the winter water had been flushed from Klondike, and replaced by a weakly stratified, warm (6–8 1C) water column with salinities of 31.5. In contrast, Burger remained well-stratified, its surface waters had warmed only slightly since the A10 survey, and there was little change in temperature and salinity of the bottom waters. However, the lower layer in Burger had thickened by 10 m and the pycnocline had shoaled (but not weakened) by nearly 10 m. The third survey (O10) included only Burger. The upper half of the water column had freshened and cooled, whereas bottom water properties registered little change.

Regional density gradients are primarily a function of salinity over the temperature ranges encountered on the surveys, with vertical salinity gradients responsible for about 2/3 of the stratification in general. The pycnocline is typically at 20–30 m and generally weakens from August through late September/early October. The sole exception to this seasonal pattern occurred in Burger in 2008, when stratification increased due to an increase in surface meltwater between August and early October. Burger

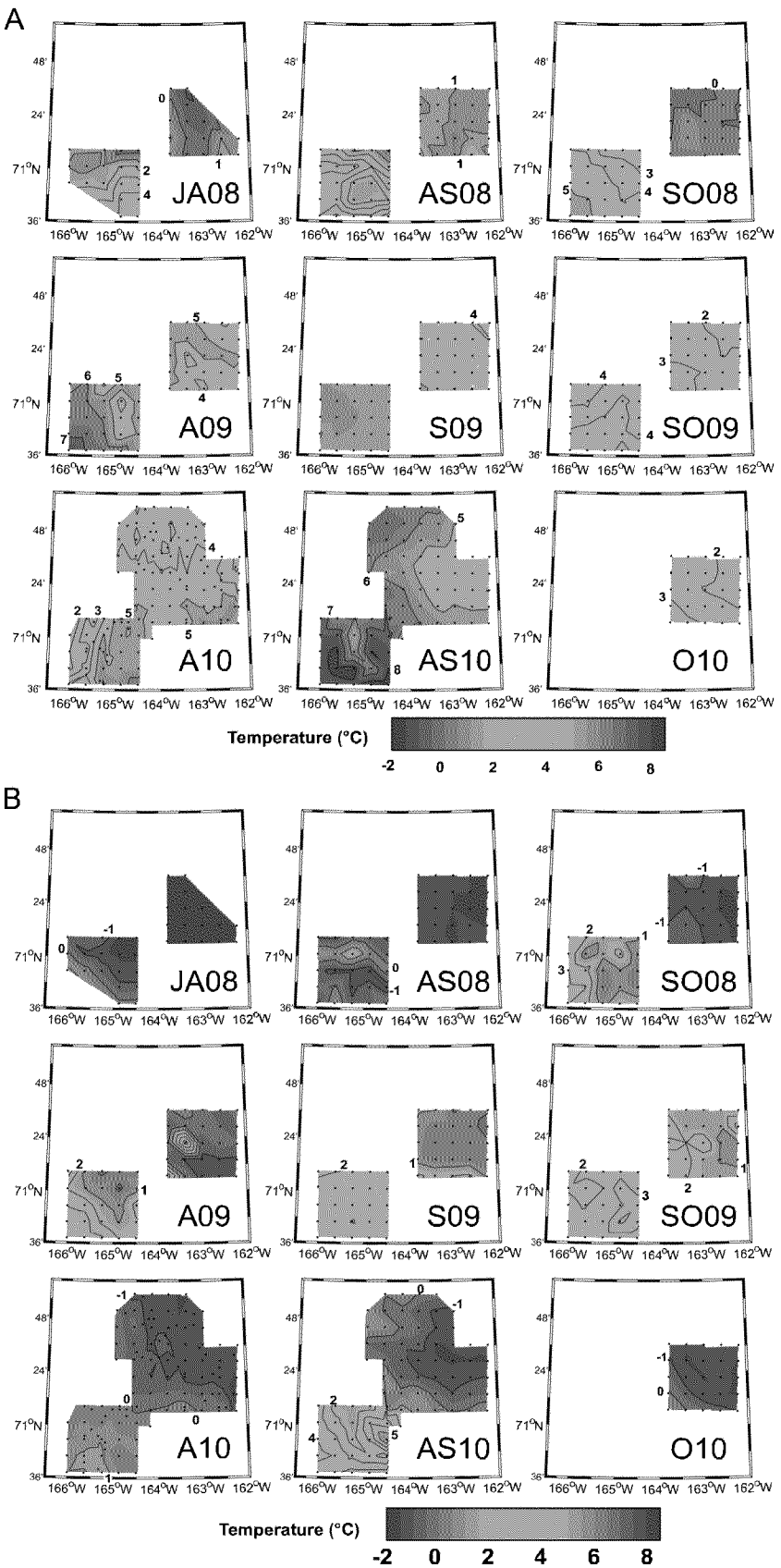

Fig. 4. (a) Plan view of temperatures averaged over the upper 10 m of the water column for each survey. Klondike is in the lower left, Burger is on the right and Statoil (2010 only) abuts Burger on the north and west. Cruise abbreviations are described in Table 1. (b). Plan view of temperatures averaged over the bottom 10 m of the water column for each survey. Klondike is in the lower left, Burger is on the right and Statoil (2010 only) abuts Burger on the north and west. Cruise abbreviations are described in Table 1.

generally consisted of meltwater in the upper water column and winter water in the lower water column so that it was more stratified than Klondike. Stratification also varied considerably among years; it was strong throughout 2008 in both areas, but moderate in 2010. By comparison the pycnocline was weaker and deeper (30 m) in September 2009.

An alternative view of the hydrography is given by plan views of the temperatures and salinities averaged over the upper and lower 10 m of the water column (Figs. 4 and 5a and b, respectively). These show that surface and bottom temperatures generally decreased from southwest to northeast across both Klondike and Burger. Over the region surface horizontal temperature gradients were as large as 5 1C (100 km)$^{-1}$ (i.e., AS10), although, more typically, these gradients were less than half this value. Bottom horizontal temperature gradients were much weaker than those at the surface. Surface salinities generally decreased from the southwest (or west) to the northeast or east. Exceptions to this tendency occurred during some of the first surveys of each year, when dilute meltwaters were present, (e.g., the A10 survey in Klondike). In contrast, bottom salinities always increase from the southwest to the northeast or east.

Bottom salinities decreased from mid-summer through fall at all sites as the saline winter-formed waters are diluted through mixing and/or replaced by advection. At the same time, surface salinities tend to increase as meltwater was removed. A prominent exception to this trend occurred in 2008, when surface salinities decreased between August and October in both Klondike and Burger. Surface waters were generally warmest during the late August–September surveys, while bottom waters were warmest in September and early October.

There are two other noteworthy features that emerged from the 2010 survey. First, the evolution of the surface and bottom temperatures and salinities in Statoil between the A10 and AS10 surveys suggest eastward movement of moderately warm, salty waters at the surface and less saline waters at depth. These changes were similar in character to those at Klondike and suggest that some fraction of the summer waters in the Central Channel flowed eastward between 70.61N and 721N (150 km). The other item of interest is the tongue of relatively cool, dilute surface waters that extend diagonally toward the southwest across a portion of Burger between the A10 and AS10 surveys, while elsewhere in Burger the surface waters became warmer and saltier. Coincident with these surface changes was the mid-depth increase in the volume of waters with temperatures o 0 1C (Fig. 3a). Note however, that this mid-depth change did not substantially change Burger bottom-water properties between the two surveys. These changes are examined in more detail later.

3.3. Heat budgets

As shown in this section, the largest seasonal changes in temperature occur in Klondike and Statoil, with both sites adjacent to and east of the Central Channel. Seasonal temperature variations in Burger, which lies south of Hanna Shoal, were smaller, especially over the lower half of the water column. These changes arise due to seasonal variations in air–sea heat exchange and differential advection of heat among sites as inferred from an examination of the heat budget.

Fig. 6 summarizes the heat budgets in terms of the control volume averaged temperature for each survey, and between-survey estimates of Q_w, Q_{as}, and Q_{oc}, which closes the budget. There are substantial spatial, seasonal, and interannual differences in each term and the mean temperatures across sites and years. Recall, that if $|Q_w|$ o 30 W m^{-2} then Q_{oc} is indeterminable (signified by "ind" in the heat budget summaries of Fig. 6).

In general, Q_{as} 4 0 (i.e., oceanic warming) in August, but becomes negative (cooling) by early to mid-September. In August, the latent and sensible heat fluxes were a source of heating or cooling, although each of these fluxes was small with average magnitudes being o 10 W m^{-2}. Both terms extract heat from the ocean in September averaging −30 W m^{-2} for Q_{latent} and −20 W m^{-2} for $Q_{sensible}$ then. $Q_{longwave}$ varied from −13 to −50 W m^{-2}, with an average value of −25 W m^{-2}. In 2009, atmospheric cooling of the ocean began in early September and was more vigorous that fall than in the other years. This early cooling was due to episodes of strong northeasterly winds that promoted vertical mixing and enhanced Q_{latent} and $Q_{sensible}$ heat losses by advecting cold air over the shelf from the northeast.

Ocean heat flux convergences show considerable spatial and temporal variability. At Klondike, this term was always a source of heat, except between the first two surveys in 2008 and 2009, when it was either indeterminable or not statistically significant. In September 2009, Q_{oc} was relatively small (39 W m^{-2}) compared to the −70 W m^{-2} of cooling by Q_{as}. By contrast, Q_{oc} was 135 W m^{-2} in September 2008, and thus solely responsible for the temperature increase between AS08 and SO08. In 2010, between the A10 and AS10 surveys, both Q_{as} and Q_{oc} added heat to the ocean at Klondike and Statoil. However, Q_{oc} was large, being 160 W m^{-2} and 137 W m^{-2} at Klondike and Statoil, respectively, and exceeded Q_{as} by a factor of 2.

There was little consistency between Q_{oc} at Burger and the other sites. In fact, Q_{oc} was only significant in two of the six cases. In both of those cases it opposed the heating or cooling tendency due to Q_{as}. Of particular interest is the fact that between A10 and AS10, Q_{oc} for Burger was −86 W m^{-2}, whereas Q_{oc} was 160 W m^{-2} for Klondike and 137 W m^{-2} for Statoil. This negative Q_{oc} flux at Burger was manifested by the increase in the volume of subsurface waters o 0 1C between A10 and AS10 evident in Burger (Fig. 3a.). It is also reflected in a section that extended from the southeast corner of Burger to the northwest corner of Statoil (Fig. 7). In comparison to the A10 sections, both AS10 sections indicate a much larger area of water enclosed by the 0 1C and −1 1C isotherm in Burger. As suggested below, this influx of winter water was probably from the northeast and it was accompanied by an 10 m shoaling the thermocline. In contrast, the warming associated with Q_{oc} at Klondike and Statoil, at approximately the same time, involved an influx of warm water over the entire depth of the water column. Although the heat budgets are crude, the differences in temperature structure and Q_{oc} are nevertheless large enough to conclude that there are considerable spatial and temporal variations in the advective heat flux among these sites.

The large Q_{oc} between A10 and AS10 for Klondike was consistent with the current and SST record obtained by the Klondike meteorological buoy for the 1 August–16 September 2010 interval. Time series of the current velocity components and SST measured at 1-m depth, along with the surface winds (Fig. 8) shows that the surface currents were generally northeastward with the record-length mean being 4 cm s^{-1} toward 491T. Although the winds varied throughout this period, on average they were westward at 4 m s^{-1}. The surface currents flowed upwind and were downwind only when westward winds exceeded 6 m s^{-1}. The mean surface velocity is similar to that observed from the Klondike current meter mooring record from 2009 discussed below. In aggregate both current meter records imply that, at least in summer, there is a strong background flow sufficient to overcome moderate surface wind stresses.

Through most of August 2010, the flow was accompanied by temperatures that varied between 2.5 1C and 6.5 1C but that generally increased through the month. However, on August 29 there was an abrupt increase in SST from 6 1C to 8 1C within a 1-day period. The mean velocity on this date was eastward at 6 c m s^{-1}, suggesting that the SST increase was due to the passage

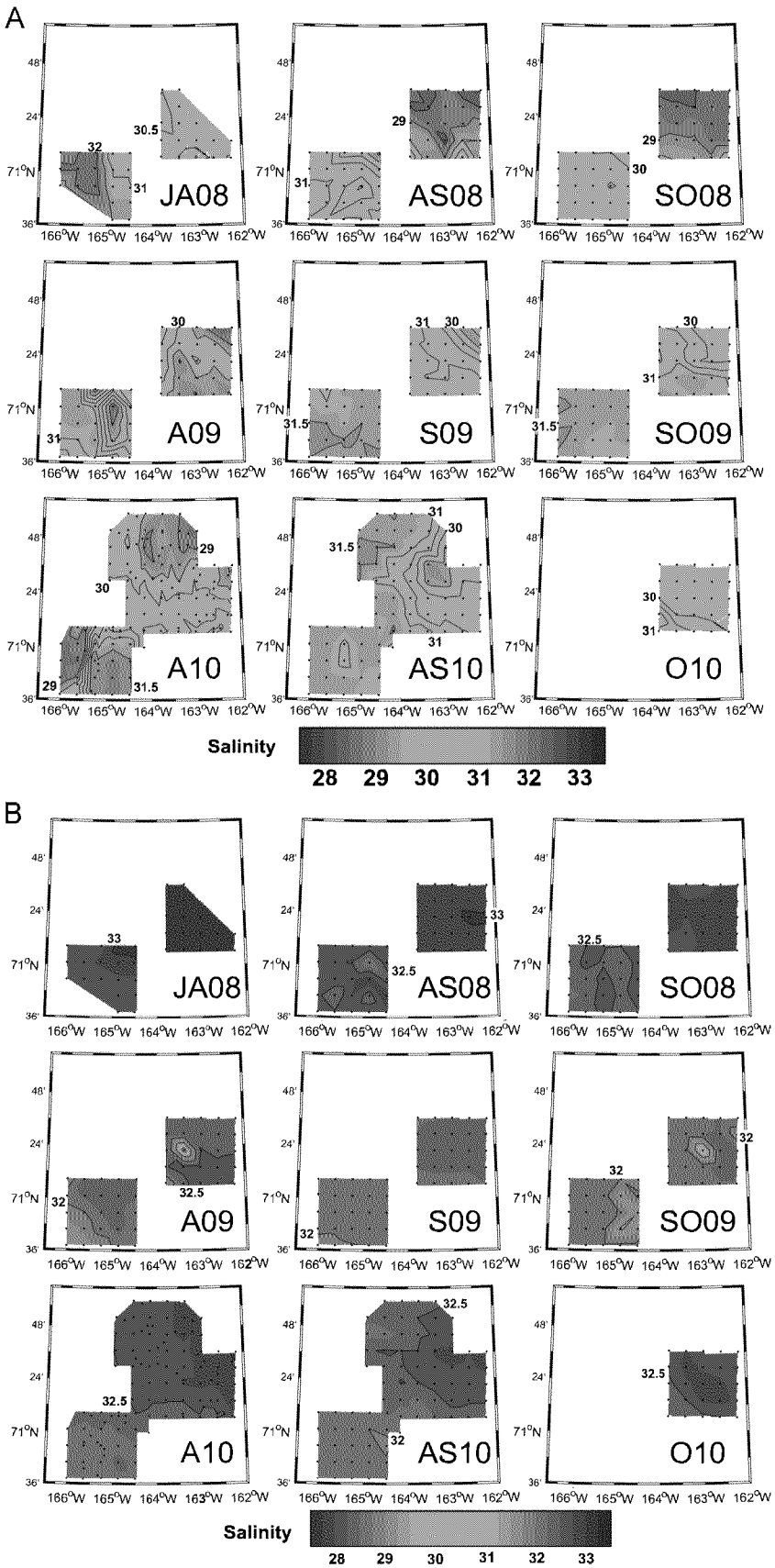

Fig. 5. (a) Plan view of salinities averaged over the top 10 m of the water column for each survey. Klondike is in the lower left, Burger is on the right and Statoil (2010 only) abuts Burger on the north and west. Cruise abbreviations are described in Table 1. (b) Plan view of salinities averaged over the bottom 10 m of the water column for each survey. Klondike is in the lower left, Burger is on the right and Statoil (2010 only) abuts Burger on the north and west. Cruise abbreviations are described in Table 1.

of a front having a zonal width scale of 5 km. The AS10 temperature transect (Fig. 3a) indicates that the 8 1C water extended to 15 m depth. Below this depth, temperatures were cooler (4 1C), although much warmer than water at similar depths to the northeast. The large Q_{oc} observed at Klondike in 2010 is consistent with these observations.

The mechanism underlying the cooling in Burger induced by Q_{oc} between A10 and AS10 is less obvious. HFR current maps (Fig. 9) for this period indicate consistently eastward, northeastward, or northward surface flow, and although the radar mask does not encompass Burger, it suggests a quasi-uniform surface flow field for the region north of 711N and west of 1611W. This flow should advect warm and comparatively salty (surface) water into Burger from the southwest. Indeed, the average temperature and salinity increased by 0.5 1C and 0.1 within the upper 5 m of Burger during this period. Quite plausibly Q_{as} could account for the surface warming. The surface salinity increase could be due to vertical mixing, but in that case we would expect a concomitant reduction in pycnocline strength between the two surveys, and this was not observed. We suggest that the surface flow advected higher salinity water into at least a portion of Burger and, in concert with Q_{as}, warmed the upper few meters of the ocean. The source of the cold intrusion at depth must then be from the north or the east of Burger, implying that in this sector of Burger there was a sub-surface flow counter to the observed surface flow.

Although current meter data were not available in 2010, some support for this contention comes from the CTD data collected during the 2010 glider survey (Fig. 1b). Temperature and salinity sections from the outbound and inbound legs of this survey are shown in Fig. 10a and b. As the glider moved from the southeast to northwest on the outbound leg, near surface temperatures and salinities decreased. However, at depths 4 10–20 m, the entire section contained cold, salty (T≤−1 1C, S≥33) water in the region east of Burger. From August 10–16 the glider moved southward along the eastern side of Burger. Along this leg, waters deeper than 20 m remained cold, but salinities gradually decreased. Upon exiting Burger, the glider veered inshore and crossed a sharp thermal front (at 100 km; Fig. 10b) where deep (4 20 m) temperatures increased by nearly 6 1C over 20 km and where surface salinities increased from 31 to nearly 32.

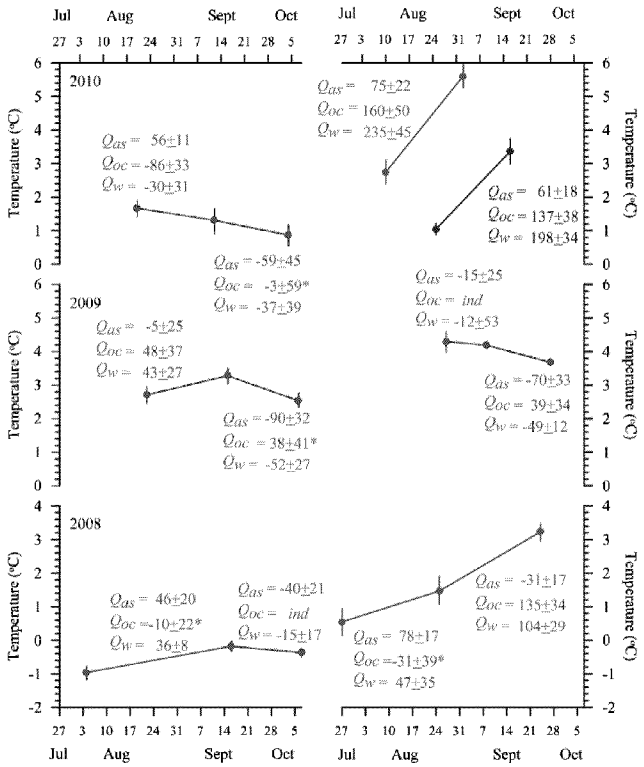

Fig. 6. Mean temperatures and heat budget summaries between each sampling period for the control volumes defined by Burger (blue), Klondike (red), and Statoil (green). Units of the heat budget are W m^{-2}. Note the difference in range of the temperature axes between 2008 and the other years. Asterisks imply that Q_{oc} is not significant at the 95% confidence level. Q_{oc}¼"ind" implies that oceanic advection cannot be assessed due to uncertainty in Q_w. (For interpretation of the references to color in this figure legend, the reader is referred to the web version of this article.)

3.4. Currents

Time series of the meridional (V) and zonal (U) components of velocity at Klondike, Burger, and Crackerjack and the NARR wind velocity components in Klondike (71.11N, 165.11W) for 1 August–6 October 2009 are plotted in Fig. 11 and summary statistics given in Table 3. The plots include the near-surface record (7 m depth) and the average of the two deep (23 m and 35 m) records, since there was little difference between these two.

For this period, the average winds were weak (1 m s^{-1}), southwestward (2481T), and not significantly different from zero at the 95% confidence limit (Table 3). The mean currents at Crackerjack (within the Central Channel) were north-northeastward at 5 cm s^{-1}, while those at Klondike were eastward at 4 cm s^{-1}. At both sites, there was little current shear between the near- and sub-surface currents both on average and through time. By contrast, the flow at Burger was vertically sheared, with southward flow of 5 cm s^{-1} near the surface and southeastward flow of 10 cm s^{-1} at depth. Although the mean flows were modest, current speeds of 10–20 cm s^{-1} were common

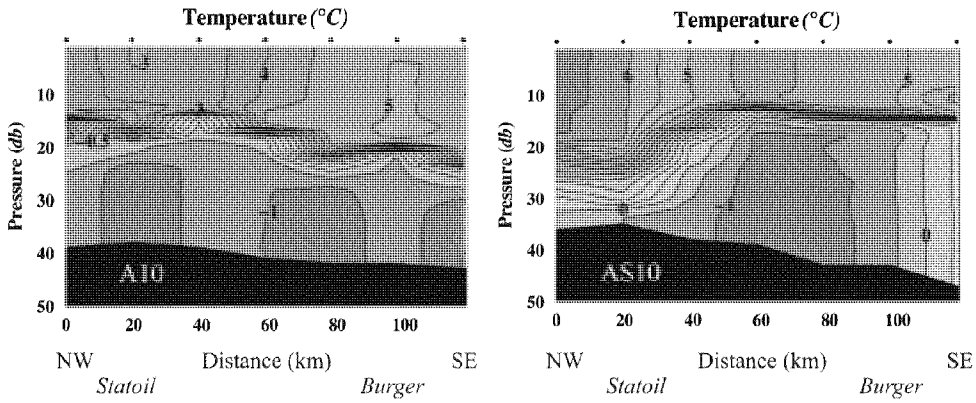

Fig. 7. Temperature cross-section running diagonally from the northwest corner of Statoil to the southeast corner of Burger from the A10 (left) and AS10 (right) surveys. CI¼0.5 1C. Cruise abbreviations are described in Table 1.

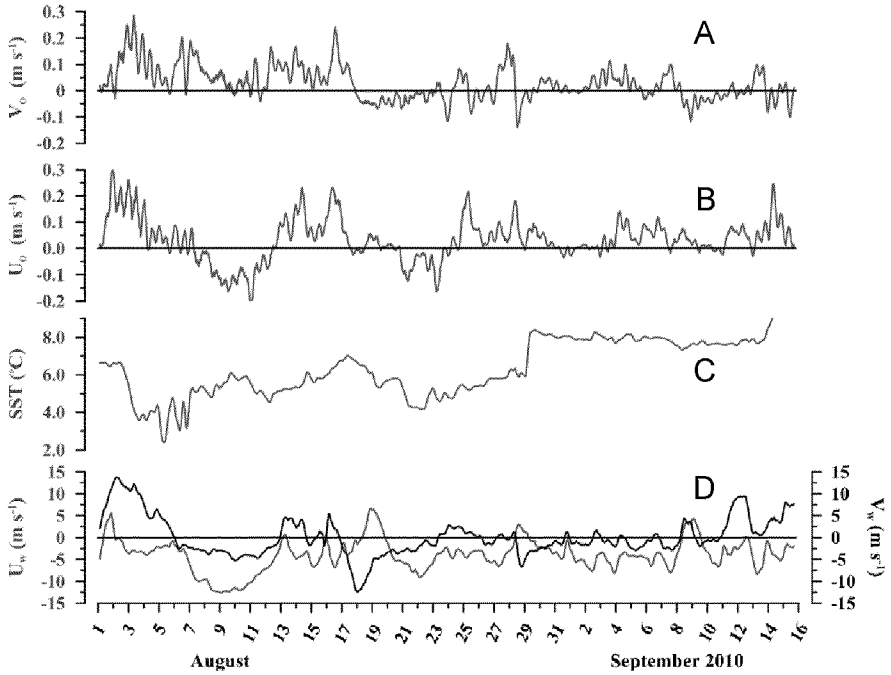

Fig. 8. Time series of the (A) meridional (V_O), (B) zonal (U_O) ocean velocity components, (C) sea surface temperature, and (D) meridional (V_W, black) and zonal (U_W, red) wind velocity components measured at the meteorological buoy in Klondike from 1 August 1 to 16 September 2010. (For interpretation of the references to color in this figure legend, the reader is referred to the web version of this article.)

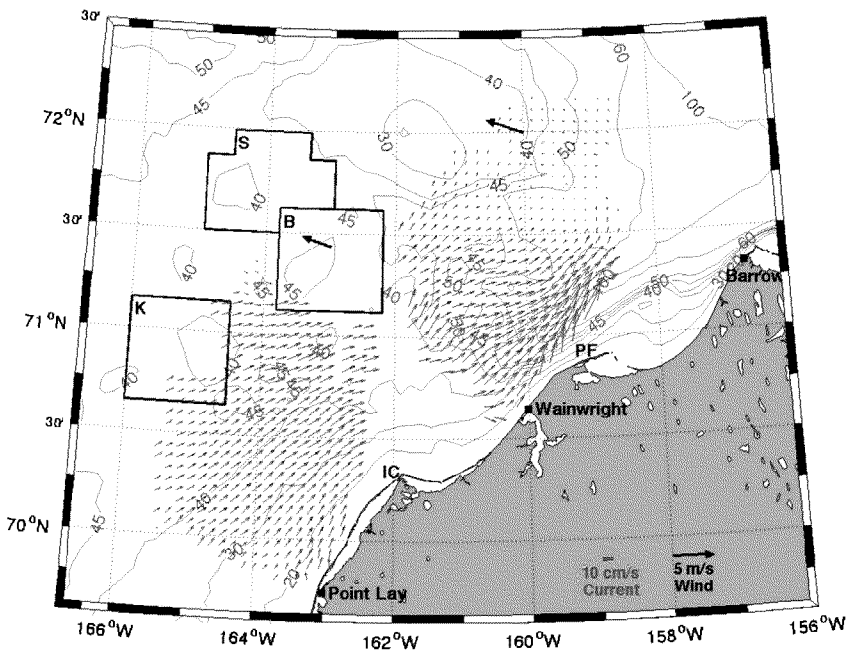

Fig. 9. Mean surface currents obtained from HFR installations at Barrow, Wainwright, and Pt. Lay. The black vectors denote the mean winds at two NARR grid points. The blue vectors denote surface currents derived from HFR at Wainwright and Barrow. The wind and blue current vectors are averages for the 12 August–17 September 17, 2010 period. The red current vectors are averages for the 13–17 September period after the HFR was installed at Point Lay. Gaps in coverage are associated with land at Icy Cape (IC) and Point Franklin (PF), which inhibit signal propagation northward from these locations. The study areas Klondike (K), Burger (B), and Statoil (S) are outlined.

with maximum values of 40 cm s^{-1} observed at Klondike and Burger over a 2-day period in early September.

Comparison of the mooring records at Klondike and Burger from September 8 to the end of the record is also of interest. During this time the mean flow at all depths in Klondike was northward at 3 c m s^{-1} (Table 3) and presumably accounted for the Q_{oc} of 39 W m^{-2} (Fig. 6). At Burger, the surface flow was southward at 5 cm s^{-1}, while the deeper flow was southeastward at 10 cm s^{-1}. For roughly the same time period, the HFR surface currents (Fig. 12) were southwestward along the east side of Hanna Shoal and then veered westward toward Burger south of 71.51N. If the surface water properties in this region were cool and fresh (as they were during the 2010 glider survey), this flow would have cooled and freshened the surface at Burger. Indeed such a response was observed here between S09 and SO09 (Figs. 4–6a and b). However during the same period, salinities decreased and temperatures increased at depth in Burger consistent with the notion of a subsurface southeastward flow advecting BSW into the southern portion of Burger.

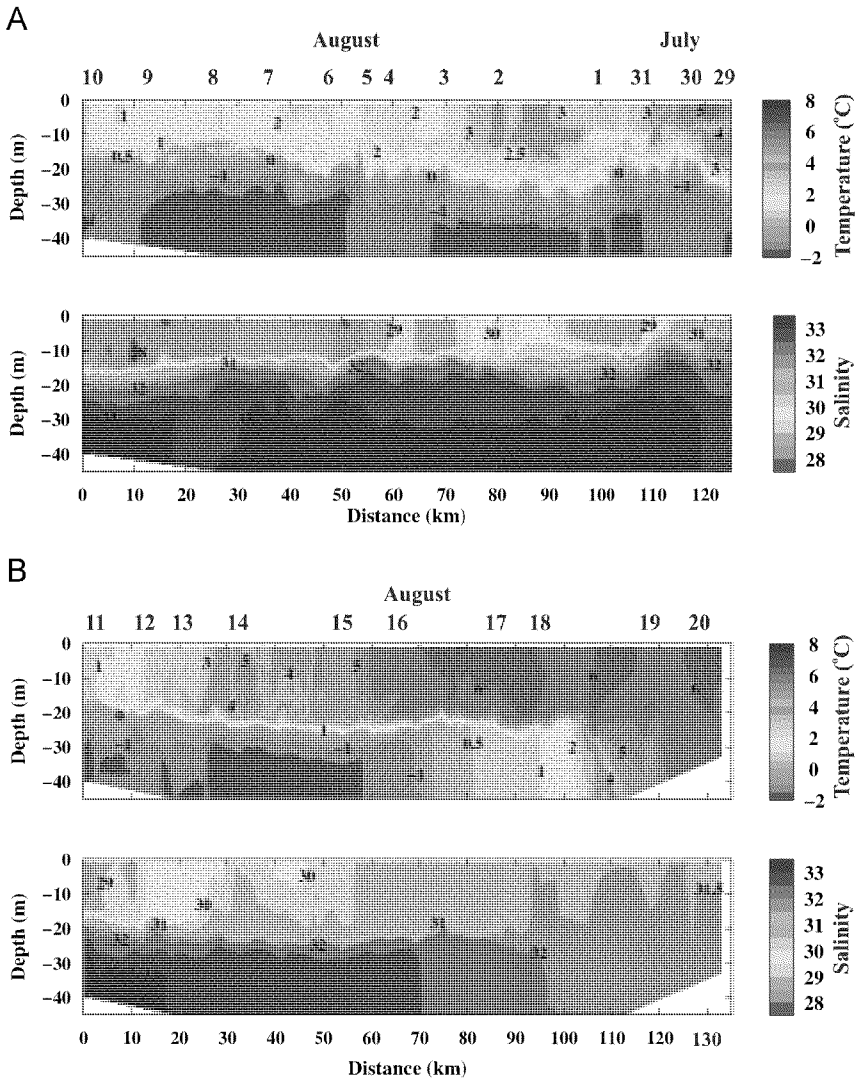

Fig. 10. Temperature and salinity sections from the 2010 glider survey along the: (A) 29 July–10 August outbound and (B) 10–20 August inbound legs. The southeast (northwest) corner of each section is on the left (right).The glider path is shown on the map in Fig. 1b.

As a final point, we note that the time series of the near-bottom temperature records in 2009 (not shown) indicate that temperatures increased from the near freezing point (−1.8 1C) to 0 1C o n 2 3 J u y l(a t Crackerjack), 1 August (at Klondike) and 26 August (at Burger) suggesting that warming of near-bottom waters progressed from west to east across the shelf. Both the mean currents and these differential rates of near-bottom temperature changes are consistent with the preceding inferences and those of Weingartner et al. (2005). They suggested that some of the water transported northward through the Central Channel moves eastward (or northeastward) across the central shelf and then toward the Alaskan coast with this flow gradually replacing near-bottom winter waters with summer waters from the Bering Sea. Note also that for the mean velocities at Burger and Klondike an oceanic heat flux convergence of 100 W m^{-2} over a 40 m deep water column requires a vertically-averaged horizontal temperature gradient of 1 1C per 100 km. These gradients are not atypical for the region and so the highest values of Q_{oc} (Fig. 6) appear reasonable.

3.5. Momentum balances

The mooring data also allow us to approximate the vertically-integrated zonal and meridional momentum balances from which we may estimate pressure gradients that drive the circulation. Our analysis assumes a small ($\ll 1$) Rossby number, which seems valid as there is no evidence of large horizontal velocity gradients over this portion of the shelf. Hence we evaluate:

$$\text{Zonal}: \frac{\partial U}{\partial t} - fV = -\underbrace{\frac{1}{\rho_0 h}\int_{-h}^{\eta}\frac{\partial p}{\partial x}dz}_{PGF_x} + \frac{\tau^x}{\rho_0 h} - \frac{rU}{h}$$

$$\text{Meridional}: \frac{\partial V}{\partial t} + fU = -\underbrace{\frac{1}{\rho_0 h}\int_{-h}^{\eta}\frac{\partial p}{\partial y}dz}_{PGF_y} + \frac{\tau^y}{\rho_0 h} - \frac{rV}{h}$$

where U (V) is the depth-averaged zonal (meridional) velocity and x (y) is the zonal (meridional) coordinate, h is the water depth, f is the Coriolis frequency evaluated at each site, t is time, η is the sea surface, ρ_0 is a reference density (1024 kg m^{-3}), and r ($=10^{-4}$ m s^{-1}) is the bottom friction coefficient (e.g., Brink, 1998). (Setting r to the high value of 5×10^{-4} m s^{-1} does not alter our conclusions.) All terms were evaluated using daily means. The surface zonal (meridional) wind stresses, τ^x(τ^y), were computed from the 3-h NARR winds following Large and Pond (1981) and then averaged into daily means. We evaluated all terms except the vertically integrated pressure gradient forces (PGF_x and PGF_y), which are the residuals in the balances. Time series of each term are plotted in Fig. 13a–c for Crackerjack, Klondike, and Burger, respectfully, and summary statistics are given in Table 4. Not

surprisingly, the results indicate approximate geostrophic balance at all locations over most of the record. Upon time-averaging, the Coriolis accelerations (and the PGFs) are more than an order of magnitude larger than the other terms. Similarly, the standard deviations of the Coriolis accelerations are also much larger than those for the other terms. For all but one of the balances, the Coriolis accelerations and the PGFs are significantly different from zero and the only ageostrophic term not significantly different from zero is bottom friction. At Burger, this term is non-zero in both the meridional and zonal balances, whereas it is non-zero for only the meridional (zonal) balance at Klondike (Crackerjack). None of the terms in the zonal momentum balance at Klondike were significantly different from zero.

The vertically-integrated pressure gradients consist of a barotropic component (associated with sea surface slopes) and a baroclinic component due to horizontal density gradients. Estimates of the geostrophic shear from the hydrographic data suggest that the baroclinic component may, on occasion, account for as much as 25% of the mean pressure gradient. However, in the absence of density gradient time series, we assume that the PGFs are solely barotropic and then estimate the average sea surface slope at each mooring site. For Crackerjack, the sea surface is inclined downward toward the northwest (298°T) with a slope of 7 cm (100 km)$^{-1}$, at Klondike it slopes downward to the north at 6 cm (100 km)$^{-1}$, and for Burger the slope tilts downward toward the northeast (43°T) with a magnitude of 11 cm (100 km)$^{-1}$.

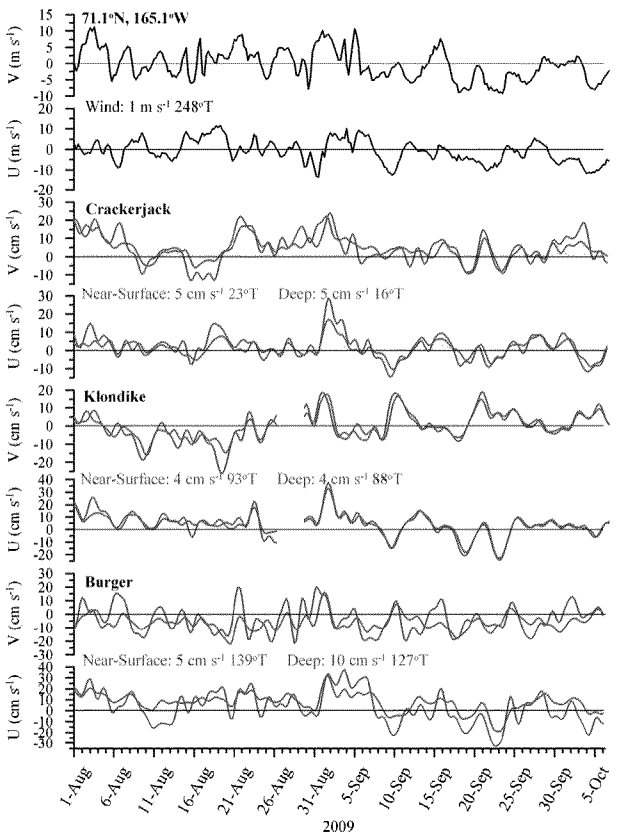

Fig. 11. Time series from 1 August–6 October 2009 of the zonal (U) and meridional (V) components of winds (topmost two panels) and currents at Crackerjack, Klondike and Burger. Near-surface (7 m) currents are in blue and the deep currents (the average at depths of 23 m and 35 m are in red). The record length mean currents are given for each depth and mooring. (For interpretation of the references to color in this figure legend, the reader is referred to the web version of this article.)

4. Discussion

We have used a variety of data sets to describe the summer-fall evolution and spatial variability in temperature and salinity properties over the central portion of the northeastern Chukchi Sea shelf (specifically the region south of Hanna Shoal and east of the Central Channel). In early August, the lower half of the water column consists of cold, high salinity waters formed during the previous winter, whereas the upper half contains cool, dilute meltwater and/or warmer and moderately saline BSW that recently arrived from Bering Strait. Through mid-August, surface waters warm, primarily through solar heating, and become saltier as meltwaters are advected out of the region and replaced by BSW. At the same time, cold, salty bottom waters are gradually replaced by these warmer but less saline waters. As a consequence of these advective influences, vertical stratification generally weakens from August through September. Between late August and mid-September air–sea heat exchanges cool the ocean, so that the oceanic heat flux is the sole source of heat to the region. The oceanic heat flux continues well into October, at least, and so is important in delaying the ice formation over the northeastern shelf (Weingartner et al., 2005). Thus in late summer and early fall both the heat budget and stratification processes over the northeastern Chukchi shelf are fundamentally three-dimensional. (On spatial scales smaller than examined here Timmermans and Winsor (2013), suggest that horizontal re-stratification associated with the slumping of meltwater fronts may also be important.)

The eastward progression of the warming signal observed in August and September 2010 implies that some of the BSW moving

Table 3
Means and standard deviations (in parentheses) for current and wind velocity components for the 1 August–6 October 2009 period at Klondike, Burger, Crackerjack and the Klondike NARR wind gridpoint (71.061N, 165.061W). Winds were southwesterly from 8/1 to 9/7 and northeasterly from 9/8 to 10/6. Italicized entries indicate significance at the 95% level. Units for currents (winds) are cm s^{-1} (m s^{-1}).

	8/1–9/7/09				9/8–10/6/09				8/1–10/6/09			
	Surface		Sub-surface		Surface		Sub-surface		Surface		Sub-surface	
	U	V	U	V	U	V	U	V	U	V	U	V
Burger	10 (13)	−3 (10)	12 (6)	−6 (6)	−6 (12)	−5 (9)	−2 (8)	−5 (5)	3 (15)	−4 (10)	8 (8)	−6 (6)
Net	11 to 107°T		13 to 118°T		7 to 230°T		6 to 154°T		5 to 180°T		10 to 127°T	
Klondike	8 (8)	−3 (8)	8 (6)	−2 (6)	−1(9)	4 (6)	−0 (8)	3 (6)	4 (8)	0 (7)	4 (7)	0 (6)
Net	8 to 112°T		8 to 106°T		4 to 344°T		3 to 354°T		4 to 93°T		4 to 88°T	
Crackerjack	4 (6)	6 (9)	2 (4)	6 (7)	−1 (6)	3 (6)	0 (5)	2 (4)	2 (7)	5 (8)	1 (4)	5 (6)
Net	7 to 34°T		7 to 19°T		3 to 344°T		2 to 4°T		5 to 23°T		5 to 16°T	
Winds	1 (5)	2 (4)			−4 (4)	−3 (4)			−1 (5)	0 (5)		
Net	2.3 to 38°T				4.8 to 232°T				1 to 248°T			

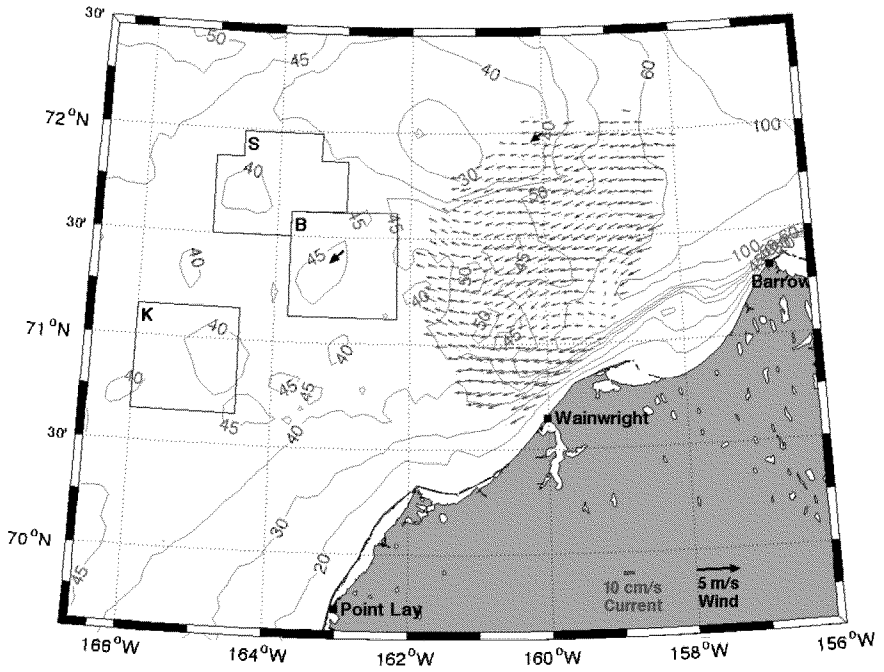

Fig. 12. Mean surface currents obtained from HFR installations at Barrow and Wainwright, in September 2009. The black vectors denote the mean winds at two NARR grid points. The blue vectors denote surface currents derived from HFR at Wainwright and Barrow. The averaging period was 13–30 September 2009. The study areas Klondike (K), Burger (B), and Statoil (S) are outlined.

northward through the Central Channel spreads eastward along the entire 150 km length of the channel bordered by the study areas. The data collected during A10 and AS10 suggests that more than half of the volume of the Statoil and Klondike survey sites was replaced over the 23 days between these surveys. After integrating along the 150 km channel length and over a 40 m deep water column, the volume change implies an eastward transport of 0.1 Sv from the Central Channel, with this water flowing at an average speed of 2 cm s^{-1}. This estimate is consistent with the mean eastward flow of 4 cm s^{-1} measured by the Klondike mooring in summer and fall 2009. Weingartner et al. (2005) suggested that on annual average 0.2 Sv may be flowing northward through the Central Channel. Although both transport estimates are crude, together they suggest that a sizeable fraction of the channel transport may be lost to the east before it reaches the outer shelf west of Hanna Shoal. This eastward transport should eventually contribute to the outflow in Barrow Canyon.

Circulation models (Winsor and Chapman, 2004; Spall, 2007) indicate that as this eastward flow moves across the central shelf toward the coast, it converges along the southern portion of Burger. This result is consistent with the mean currents measured at the Burger mooring for the August to early October period in 2009. Here, the flow in the lower half of the water column was 10 cm s^{-1} to the east-southeast, nearly twice that of Klondike during the same period. In both models, this convergence is reflected in the streamlines which wrap clockwise around the northern and southeastern sides of Hanna Shoal. From here, some of the model streamlines continue to the southwest before retroflecting eastward toward the Alaskan coast. The models' retroflection point appears to occur in the vicinity of Burger.

Our observations indicate that water properties in Burger are generally quite different than those at Klondike and Statoil. In particular, meltwaters are more prevalent and dense bottom waters remain in Burger much longer than at the other sites. There may be several reasons for the greater persistence of winter water at Burger. First, it may simply reflect the longer time required for BSW to move eastward from the Central Channel and flush the waters from Burger. Second, the models suggest that, on average, dense winter water from the east side of Hanna Shoal is fed into Burger. This is consistent with our inference that oceanic advection cooled Burger between the A10 and AS10 surveys. It is also consistent with the observed increase in the volume of cold waters seen at depth in the sections shown in Figs. 4a and 8, suggesting the source of this cold water was north or northeast of Burger. Finally, we note that dense cold pools, underlying a less dense surface layer, may be inherently stagnant features on shallow continental shelves (Hill, 1996). The near-bottom baroclinic circulation attendant with such pools tends to spin down rapidly over a few days due to bottom friction, leaving the flow concentrated in the surface layer. Although our observations cannot determine which of these mechanisms is dominant, all may contribute to the persistence of dense bottom waters in Burger. Whether operating in aggregate or independently, convergence and/or stagnant bottom flow in the northeast corner of Burger could result in higher carbon deposition rates here compared to Klondike and Statoil. Similarly, the prevalence of surface meltwaters at Burger is consistent with the first two mechanisms. Moreover, because meltwater probably resides over Hanna Shoal through much of summer, northerly winds may quickly advect this water into Burger, enhancing the stratification here relative to the other sites. We conclude that Burger receives different water masses at the surface and at depth in summer. At depth this includes Bering Sea Water from the west and winter water from the northeast. The surface circulation may alternately contribute dilute, cool meltwaters from the northeast or warmer, more saline waters from the south. However, it is not completely clear how these differential fluxes compete over time and across Burger. As shown by the other papers in this issue, there are distinct biological attributes between Burger and the other sites (Blanchard et al., 2013a, 2013b; Questel et al., 2013; Norcross et al., 2013), with these differences plausibly attributed to variations in water properties, stratification, and carbon deposition rates that are a consequence of the circulation dynamics.

We have used the current meter data to estimate the momentum balance over the central shelf. The flow is predominantly a balance between the Coriolis accelerations and barotropic

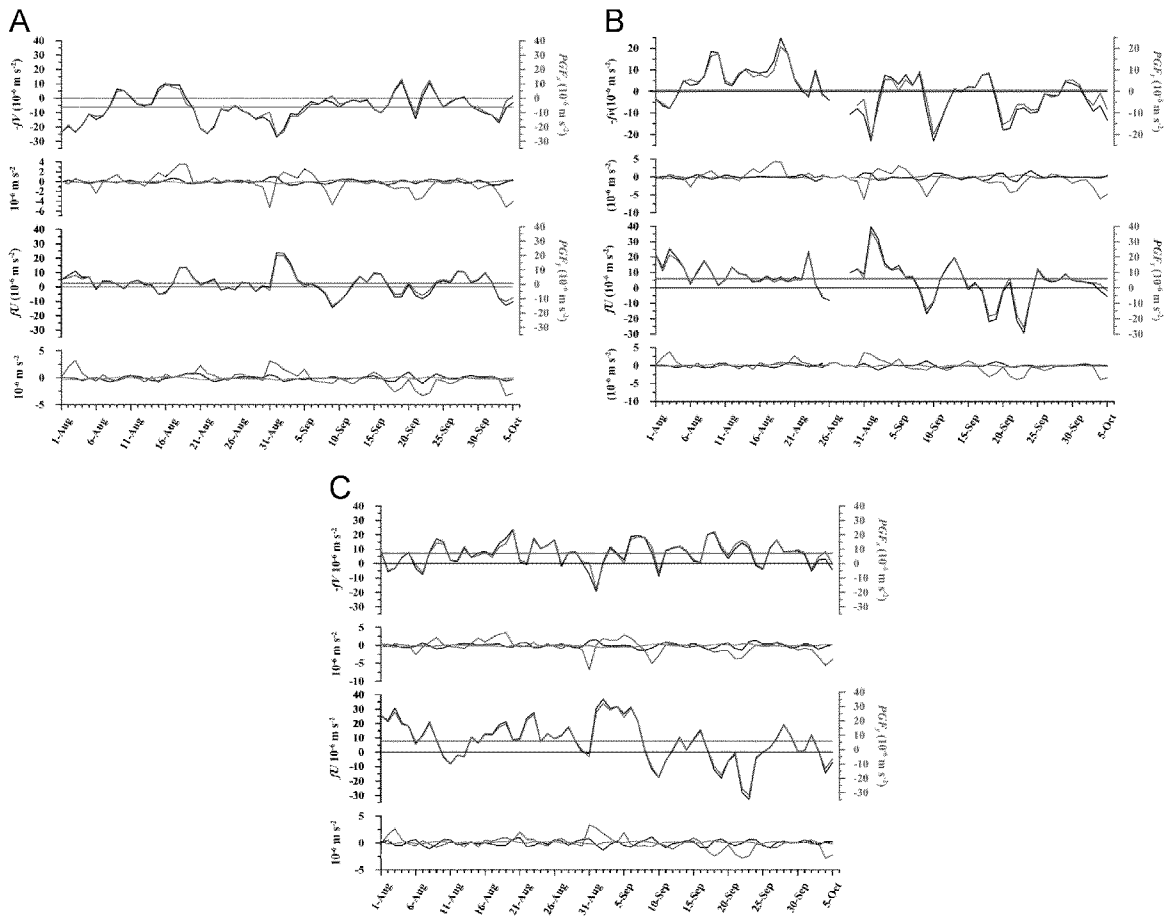

Fig. 13. (a) Time series from 1 August–6 October 2009 of the terms comprising the zonal (two upper panels) and meridional (two lower panels) momentum balances for Crackerjack. The terms in the geostrophic balance are plotted separately from the other terms for clarity. The other terms are local acceleration (black), bottom friction (magenta), and wind stress (red). For the geostrophic terms the Coriolis acceleration is black and the pressure gradient force is blue. The horizontal blue line in the geostrophic balance plots is the mean pressure gradient force. (b) Time series from 1 August–6 October 2009 of the terms comprising the zonal (two upper panels) and meridional (two lower panels) momentum balances for Klondike. The terms in the geostrophic balance are plotted separately from the other terms for clarity. The other terms are local acceleration (black), bottom friction (magenta), and wind stress (red). For the geostrophic terms the Coriolis acceleration is black and the pressure gradient force is blue. The horizontal blue line in the geostrophic balance plots is the mean pressure gradient force. (c) Time series from 1 August–6 October 2009 of the terms comprising the zonal (two upper panels) and meridional (two lower panels) momentum balances for Burger. The terms in the geostrophic balance are plotted separately from the other terms for clarity. The other terms are local acceleration (black), bottom friction (magenta), and wind stress (red). For the geostrophic terms the Coriolis acceleration is black and the pressure gradient force is blue. The horizontal blue line in the geostrophic balance plots is the mean pressure gradient force. (For interpretation of the references to color in this figure legend, the reader is referred to the web version of this article.)

pressure gradients because all other terms in the momentum balance, except bottom friction, were not statistically different from zero. Mean sea-surface slopes range from 6 cm to 10 cm $(100\ km)^{-1}$ over the central shelf and slope downward to the northwest at Crackerjack, to the north at Klondike, and to the northeast at Burger. The magnitudes of these slopes are comparable with estimates of the mean sea surface slope of 5–10 cm $(100\ km)^{-1}$ between the Pacific and Arctic oceans (Coachman et al., 1975; Stigebrandt, 1984; Aagaard et al., 2006). Our mean sea surface slope estimates were computed over a period of time when the mean wind stress was negligible, hence these values may be useful for comparison with results from numerical models subject only to the inflow through Bering Strait. They also provide a useful benchmark for comparison with other seasons when the surface stress may be larger due to stronger winds and/or drifting sea–ice.

There were also considerable year-to-year differences in ocean temperature distributions at the time of the first surveys. In 2008, average early August temperatures were −1 1C in Burger and 0.5 1C in Klondike. In comparison, mid-August 2009 (2010) temperatures were nearly 3 1C (2 1C) at Burger and 4 1C (2.7 1C) at Klondike. While some of this variation may arise due to differences in local Q_{oc} prior to the initial survey dates in each year, they are not due to year-to-year variations in Q_{as}. Throughout summer, net solar radiation is the largest positive component of Q_{as}. For the three years considered, interannual differences in the mean daily June–July net incoming and albedo-corrected solar radiative flux (based on Barrow ARM measurements) were: 178 W m^{-2} (2008), 181 W m^{-2} (2009), and 196 m^{-2} (2010). These differences are small and result in a maximal temperature difference of only 0.7 1C when integrated over a 40 m deep water column after two months of solar heating at the given rates. Instead it appears that much of the interannual temperature variability early in the season is associated with processes occurring farther south and/or with the winds. The former suggestion is supported by satellite thermal imagery for the region between 166–1701W and 68–691N (denoted by the box in Fig. 1a). We averaged all available thermal images in this box over the 3–12 July interval of each year. (These dates were the only ones for which these data were available in each year for such a comparison). In 2008, the mean SST was 3.7 1C, while the comparable means in 2009 and 2010 were 5.4 1C and 5.2 1C, respectively. Most likely the temperature differences among years were established over the Bering Sea shelf and advected northward into the Chukchi Sea. Winds were also considerably different in each year. For example, in 2008 mean monthly winds for August and September were northeasterly (3 m s^{-1}) on average over the northeastern shelf and relatively

Table 4
Statistics for the terms in the Burger, Klondike, and Crackerjack momentum balances for the 1 August 1–6 October 2009 period. Bold-faced values are statistically significant at the 95% confidence level. Units are in 10^{-6} m^2 s^{-1}, s is the standard deviation, and CI is the 95% confidence interval on the means.

	Burger ZONAL					Burger MERIDIONAL				
	$\partial U/\partial t$	$-fV$	$\tau^x/\rho_0 h$	rU/h	PGF_x	$\partial V/\partial t$	fU	$\tau^y/\rho_0 h$	rV/h	PGFy
Min	−1.40	−19.42	−6.81	−0.60	−17.50	−1.3	−32.73	−2.86	−0.31	−29.82
Max	1.58	23.83	3.55	0.53	23.33	1.12	37.08	3.4	0.38	33.98
Mean	−0.04	6.70	−0.43	−0.13	7.23	0.008	7.84	−0.04	0.11	7.78
s	0.65	8.45	1.93	0.24	7.73	0.53	14.65	1.21	0.14	13.67
CI	0.19	2.47	0.56	0.07	2.26	0.15	4.28	0.35	0.04	4.00
	Klondike ZONAL					Klondike MERIDIONAL				
	$\partial U/\partial t$	$-fV$	$\tau^x/\rho_0 h$	rU/h	PGF_x	$\partial V/\partial t$	fU	$\tau^y/\rho_0 h$	rV/h	PGFy
Min	−1.38	−22.95	−6.34	−0.74	−21.75	−1.27	−29.28	−3.93	−0.43	−25.68
Max	1.73	24.78	4.22	0.54	20.69	1.31	39.66	3.83	0.46	36.68
Mean	−0.048	0.19	−0.42	−0.11	0.67	−0.001	5.72	−0.16	0.004	5.87
s	0.60	8.46	1.98	0.21	7.5	0.46	11.33	1.51	0.16	10.25
CI	0.18	2.51	0.59	0.06	2.2	0.14	3.36	0.45	0.05	3.04
	Crackerjack ZONAL					Crackerjack MERIDIONAL				
	$\partial U/\partial t$	$-fV$	$\tau^x/\rho_0 h$	rU/h	PGF_x	$\partial V/\partial t$	fU	$\tau^y/\rho_0 h$	rV/h	PGF_y
Min	−0.79	−26.95	−5.37	−0.38	−26.13	−1.04	−14.41	−3.33	−0.42	−13.12
Max	1.00	11.66	3.58	0.22	13.16	1.09	23.95	3.25	0.18	21.96
Mean	−0.02	−6.54	−0.35	−0.03	−6.18	−0.02	2.31	−0.11	−0.10	2.50
s	0.38	9.14	1.77	0.12	9.09	0.41	7.40	1.33	0.14	6.73
CI	0.11	2.67	0.52	0.04	2.65	0.12	2.16	0.39	0.04	1.97

steady. The mean winds in 2009, were southwesterly in August and northeasterly in September. In 2010, the winds were easterly or southeasterly in both months at 2 m s^{-1}. The preponderance of winds from the northeast in 2008 would retard meltwater removal from the region and, perhaps also, the seasonal displacement of dense bottom waters. This suggestion is consistent with the HFR measurements and the Burger current meter record in September 2009 (Fig. 12), during which time the surface flow was southwestward when the winds were from the northeast.

As a final comment, we note that the spring sea–ice distribution and its subsequent evolution differed considerably among the years sampled. In 2008 and 2010, open water first appeared in early May in the northeastern Chukchi Sea and then spread westward from the Alaskan coast in an apparent response to easterly winds. Meanwhile, Bering Strait and the southern Chukchi Sea remained ice-covered until late May. In contrast, ice in 2009 began retreating northward from Bering Strait in early May, with this retreat pattern maintained through late June. However, only in late June did ice begin to retreat westward across the northeastern shelf following a burst of easterly winds. Although these early differences in ice retreat were striking, they were not prominently reflected in subsequent temperature and salinity differences, nor do they appear to be good predictors of the ice cover in late July or early August. For example, ice began retreating early in 2008, but the retreat stalled over the northeast shelf from mid-July through August as winds blew steadily from the northeast. The collapse of the ice retreat likely resulted in the relatively large volumes of meltwater over the study region in 2008. In contrast, although ice retreat over the northeastern shelf occurred much later in 2009, this delay was not reflected in an inordinate amount of cool, dilute meltwater.

Although August temperature and salinity properties of the water column did not appear sensitive to the springtime evolution of sea–ice retreat, biological production may be significantly affected. Westward retreat of ice from the Alaskan coast in early May should have promoted pelagic primary production in spring 2008 and 2010. In contrast, sympagic primary production was probably the dominant mode of phytoplankton production in spring 2009. Regardless of production mode, much of the spring production is ungrazed because zooplankton abundance does not increase significantly until later in the summer (Questel et al., 2013). Thus, the timing and rates of primary production and the amount of phytoplankton biomass produced quite likely differed among these years.

5. Conclusions

Our results underscore the important role that advection of Bering Sea Water exerts on the summer and fall water properties of the central Chukchi Sea shelf as well as the processes controlling this shelf's heat budget and stratification. These processes, temperatures, and salinities vary remarkably over relatively small (50-100 km) distances across the 40–45-m deep northeastern Chukchi shelf. The spatial variations reflect potential vorticity constraints, induced by the bathymetry, on the flow. Numerical models and observations suggest that Bering Sea Water spreads eastward from the Central Channel, gradually replacing surface meltwaters and deeper winter waters from the region. On the other hand, the predicted clockwise movement of water around Hanna Shoal would tend to transport dense, winter-formed waters back into the same general area. Convergence of these different water masses may explain much of the spatial variability in observed water properties and processes. Our heat budget analysis, although crude, suggests that accurate predictions of fall ice formation requires a better understanding of the circulation and air–sea heat exchanges, since these appear to oppose one another in fall. Additional measurements are now underway to examine the regional circulation and air–sea heat exchanges in more detail.

Acknowledgements

This research was funded by ConocoPhillips Alaska Company, Anchorage, AK; Shell Exploration and Production Company, Anchorage, AK; and Statoil USA E+P, Inc., Anchorage, AK. Additional support for the glider and HFR program was provided by grants from BOEM, US Dept. of Interior, ConocoPhillips, and Shell Exploration & Production Company. We are grateful to the many people who assisted in various phases of the project, especially Caryn Rea (ConocoPhillips), Michael Macrander (Shell), and Steinar Eldøy (Statoil), Robert Day, Sheyna Wisdom, Dave Aldrich, Jeff Hastings, and the officers and crews of the M/V Bluefin, the R/V Westward Wind, and the R/V Norseman II. Robert Shears of Olgoonik Oilfield Services assisted in

the glider operations conducted from Wainwright. We thank the residents of Pt. Lay, Wainwright, and Barrow for permission to conduct HFR operations on their land and the Barrow Arctic Science Consortium for assistance with the HFR effort. Arny Blanchard provided statistical advice.

References

Aagaard, K., Weingartner, T.J., Danielson, S.L., Woodgate, R.A., Johnson, G.C., Whitledge, T.E., 2006. Some controls on flow and salinity in Bering Strait. Geophysical Research Letters 33, L19602, http://dx.doi.org/10.1029/2006GL026612.

Barrick, D.E., Lipa, B.J., Crissman, R.D., 1985. Mapping surface currents with CODAR. Sea Technology 26, 43–48.

Barrick, D.E., Lipa., B.J., 1986. Correcting for distorted antenna patterns in CODAR ocean surface measurements. IEEE Journal of Oceanic Engineering OE-11 (2), 304–309.

Berry, D.I., Kent, E.C., 2009. A new air–sea interaction gridded dataset from ICOADS with uncertainty estimates. Bulletin of the American Meteorological Society 90, 646–656.

Blanchard, A.L., Parris, C.L., Knowlton, A.L., Wade, N.R., 2013a. Benthic ecology of the northeastern Chukchi Sea. Part I. Environmental characteristics and macrofaunal community structure 2008–2010. Continental Shelf Research 67, 52–66.

Blanchard, A.L., Parris, C.L., Knowlton, A.L., Wade, N.R., 2013b. Benthic ecology of the northeastern Chukchi Sea. Part II: Spatial variation of megafaunal community structure, 2009–2010. Continental Shelf Research 67, 67–76.

Brink, K.H., 1998. Wind-driven currents over the continental shelf. The Sea 10, 3–20.

Brower, Jr., W.A., Wise, J.L., Baldwin, R.G., Leslie, L.D., Willimas, Jr., C.N., 1988. Climatic Atlas of the Outer Continental Shelf Waters and Coastal Regions of Alaska, Volume III Chukchi-Beaufort Sea. National Climate Data Center, Asheville, NC. 497 pp.

Coachman, L.K., Aagaard, K., Tripp, R.B., 1975. Bering Strait: The Regional Physical Oceanography. Univ. of Washington Press, Seattle172.

Emery, W.J., Thomson, R.E., 2001. Data Analysis Methods in Physical Oceanography Second and Revised ed., Elsevier, Inc., San Diego, CA, 638 pp.

Gall, A.E., Day, R.H., Weingartner, T.J., 2013. Structure and variability of the marine-bird community in the northeastern Chukchi Sea. Continental Shelf Research 67, 96–115.

Hill, A.E., 1996. Spin-down and the dynamics of dense pool gyres in shallow seas. Journal of Marine Research 54, 471–486.

Josey, S.A., Pascal, R.W., Taylor, P.K., Yelland, M.J., 2003. A new formula for determining the atmospheric longwave flux at the ocean surface at mid-high latitudes. Journal of Geophysical Research 108, 3108, http://dx.doi.org/10.1029/2002JC001418.

Kohut, J.T., Glenn, S., 2003. Improving HF radar surface current measurements with measured antenna beam patterns. Journal of Atmospheric and Oceanic Technology 20 2303–1316.

Ladd, C., Bond, N., 2002. Evaluation of the NCEP/NCAR reanalysis in the NE Pacific and the Bering Sea. Journal of Geophysical Research 107, C10, http://dx.doi.org/10.1029/ 2001JC001157.

Large, W.G., Pond, S., 1981. Open ocean momentum flux measurements in moderate to strong winds. Journal of Physical Oceanography 11, 324–336.

Lawrence, M., 2005. The relationship between relative humidity and the dewpoint temperature in moist air: a simple conversion and applications. Bulletin of the American Meteorological Society 86, 225–233.

Manly, B.F.J., 1997. Randomization, Bootstrap and Monte Carlo Methods in Biology. Chapman & Hall, London399.

Martin, S., Drucker, R., 1997. The effect of possible Taylor columns on the summer sea ice in the Chukchi Sea. Journal of Geophysical Research 102, 10473–10482.

Mesinger, F., Coauthors, 1.9., 2006. North American regional re-analysis. Bulletin of the American Meteorological Society 87, 343–360.

Mudge, T.D., Fissel, D.B., Kulan, N., Sadowy, D., Borg, K., Lawrence, J., Marko, J.R., Billenness, D., Hung, T., Kanwar, A., Bard, A., 2010. Analysis of Ice and Metocean Measurements, Chukchi Sea, 2009–2010. Report for ConocoPhillips Alaska Inc., Anchorage, Alaska by ASL Environmental Sciences Inc., Victoria, B.C. Canada. x+134 p.

Norcross, B.L., Raborn, S.W., Holladay, B.A., Gallaway, B.J., Crawford, S.T., Priest, J.T., Edenfield, L.E., Meyer, R., 2013. Northeastern Chukchi Sea demersal fishes and associated environmental characteristics, 2009–2010. Continental Shelf Research 67, 77–95.

Pickart, R.S., Weingartner, T., Pratt, L.J., Zimmermann, S., Torres, D.J., 2005. Flow of winter-transformed Pacific water into the western Arctic. Deep-Sea Research Part II: Topical Studies in Oceanography 52, 3175–3198.

Questel, J.M., Clarke, C., Hopcroft, R.R., 2013. Seasonal and interannual variation in the planktonic communities of the northeastern Chukchi Sea during the summer and early fall. Continental Shelf Research 67, 23–41.

Shroyer, E.L., Plueddemann, A.J. Wind-driven modification of the Alaskan coastal current. Journal of Geophysical Research 117,C03031, http://dx.doi.org/10.1029/2011JC007650, in press.

Spall, M.A., 2007. Circulation and water mass transformation in a model of the Chukchi Sea. Journal of Geophysical Research 112, C05025, http://dx.doi.org/10.1029/2005JC002264.

Spreen, G., Kaleschke, L., Heygster, G., 2008. Sea ice remote sensing using AMSR-E 89 GHz channels. Journal of Geophysical Research 113, C02S03, http://dx.doi.org/10.1029/2005JC003384.

Stigebrandt, A., 1984. The north Pacific: a global-scale estuary. Journal of Physical Oceanography 14, 464–470.

Teague, C., 2001. Ionospheric Effects on Coastal Radar Systems. Radiowave Oceanography the First International Workshop, H.C. Graber and J. D. Paduan (eds.), pp. 56–61.

Timmermans, M.L., Winsor, P., 2013. Scales of horizontal density structure in the Chukchi Sea surface layer. Continental Shelf Research 52, 39–45.

Walsh, J., Chapman, E., Portis D., W.L., 2009. Arctic cloud fraction and radiative fluxes in atmospheric re-analyses. Journal of Climate 22, 2316–2334.

Walsh, J.J., McRoy, C.P., Coachman, L.K., Goering, J.J., Nihoul, J.J., Whitledge, T.E., Blackburn, T.H., Parker, P.L., Wirick, C.D., Shuert, P.G., Grebmeier, J.M., Springer, A.M., Tripp, R.D., Hansell, D.A., Djenedi, S., Deleersnijder, S., Henriksen, K., Lund, B. A., Andersen, P., Müller-Karger, F.E., Dean, K., 1989. Carbon and nitrogen cycling within the Bering/Chukchi seas: source regions for organic matter affecting AOU demands of the Arctic Ocean. Progress in Oceanography, 22; 277–359.

Weingartner, T., Aagaard, K., Woodgate, R., Danielson, S., Sasaki, Y., Cavalieri, D., 2005. Circulation on the north central Chukchi Sea shelf. Deep-Sea Research Part II: Topical Studies in Oceanography 52, 3150–3174.

Weingartner, T.J., Cavalieri, D.J., Aagaard, D.J., Sasaki, Y., K., 1998. Circulation, dense water formation and outflow on the northeast Chukchi Sea shelf. Journal of Geophysical Research 103, 7647–7662.

Winsor, P., Chapman, D.C., 2004. Pathways of Pacific water across the Chukchi Sea: a numerical model study. Journal of Geophysical Research 109, C03002, doi: 1029/2003JC001962.

Woodgate, R.A., Aagaard, K., Weingartner, T.J., 2005a. Monthly temperature, salinity, and transport variability of the Bering Strait through flow. Geophysical Research Letters 32, L04601, http://dx.doi.org/10.1029/2004GL021880.

Woodgate, R.A., Aagaard, K., Weingartner, T.J., 2005b. A year in the physical oceanography of the Chukchi Sea: moored measurements from autumn 1990–1991. Deep-Sea Research Part II: Topical Studies in Oceanography 52, 3116–3149.

To: Conmy, Robyn[Conmy.Robyn@epa.gov]
Cc: Schubauer-Berigan, Joseph[Schubauer-Berigan.Joseph@epa.gov]
From: McClellan, Kim
Sent: Mon 8/22/2016 5:54:10 PM
Subject: Submission Return
E12PG00037_Draft Final Report_June 2016_clean copy_abg.docx

Hi Robyn,

Submission Return	Kim McClellan	Robyn.Conmy@RDC.Conmy173455	Dispersant Effectiveness, In-Situ Droplet Size Distribution and Numerical Modeling to Assess Subsurface Dispersant Injection as a Deepwater Blowout Oil Spill Response OptionandEvaluation of Oil Fluorescence Characteristics to Improve Forensic Response Tools	Report	8/18/2016 8:32 AM

I sent this last week, but I just wanted to make sure you received this Submission Return from your Report that is currently being reviewed in STICS. Alice Gilliland sent these comments:

Excellent report! Given the topic, will be routed for STICS review at the Laboratory level. Prior to my approval, I am returning this to the author with my review comments ("E12PG00037_Draft Final Report_June 2016_clean copy_abg.docx).	Alice Gilliland	08/18/2016 8:32 AM

Please make your revision to the report, email it to me and then I can resubmit it to Alice for her review and approval.

Thanks,

Kim

Studies on Dispersion Effectiveness and Droplet Size Distribution of Two Oils in Seawater

Zhong Pan[1], Lin Zhao[1], Michel C. Boufadel[1], Thomas King[2], Brian Robinson[2], Robyn Conmy[3], and Kenneth Lee[4]

[1]Center for Natural Resources Development and Protection, Department of Civil and Environmental Engineering, New Jersey Institute of Technology, Newark, NJ, 07102, USA

[2]Center for Offshore Oil, Gas and Energy Research, Department of Fisheries and Oceans Canada, Bedford Institute of Oceanography, Dartmouth, NS B2Y 4A2, Canada

[3] USEPA/NRMRL/LRPCD, 26 West MLK Drive

*Corresponding author: boudadel@gmail.com

Abstract

Alaska Northern Slope (ANS) crude oil and Cold Lake Blend (CLB) diluted bitumen were used to evaluate the effects of dispersants, mixing energy, and mixing time on the dispersibility of surface oil spilled in the baffled flask seawater mixing system. The dispersion effectiveness and oil droplet size distribution of two oils were measured under various conditions. The addition of dispersant steadily increased small ANS oil droplets with increasing mixing time. The increase in mixing energy resulted in faster formation of smaller droplets, reflecting very effective dispersion at higher mixing energy in the presence of dispersant. In contrast, limited oil dispersion occurred either exposed to high or low mixing energy without dispersant. For the CLB dispersion, relatively poorer dispersion was observed under the definite condition, which may be due to the high viscosity of CLB as opposed to that of ANS. The results showed that dispersion effectiveness and oil droplet size distribution were comprehensively controlled by the addition of dispersants, mixing energy and time, and oil viscosity. This potentially provided a robust tool to optimize these parameters for the best oil dispersion performance in response to future oil spill accidents.

Keywords: dispersion effectiveness, droplet size distribution, dispersant, mixing energy, mixing time

1. Introduction

Due to increased offshore oil production, gas exploration, and crude oil transportation from offshore platforms, oil spill accidents have occurred in the past few decades. Two worst oil spills in U.S. history, the Exxon Valdez spill in 1989 (Boufadel et al. 2010, Li and Boufadel 2010) and the BP Deepwater Horizon (DWH) spill in 2010, brought about disastrous environmental consequences (Atlas and Hazen 2011). The Exxon Valdez spill released ~42 million liters of crude oil, while the BP DWH spill released ~780 million liters of crude oil into Gulf of Mexico (Atlas and Hazen 2011, Boufadel et al. 2014, Zhao et al. 2014, Zhao et al. 2015). In response to the spills, chemical dispersion has been widely accepted as an effective mitigation technique. Unprecedented amounts (~8 million liters) of dispersant (1.1 million liters of Corexit 9527A and 6.8 million liters of Corexit EC9500A) were employed in the Gulf of Mexico to mitigate the impact of the DWH spill (Kujawinski et al. 2011, Gong et al. 2015). The dispersion effectiveness (DE) is a key parameter in determining whether to use dispersants as a spill response option (Moles et al. 2002). It is important to recognize that many factors influence dispersant performance, including oil composition and properties, mixing energy, mixing time, state of oil weathering, fluid dynamics, the type of dispersant used and the amount applied, temperature, and salinity of the water (Clayton et al. 1993, Brandvik and Daling 1998, Blondina et al. 1999, Wrenn et al. 2009, Mukherjee et al. 2011).

Oil spilled on the water surface spreads as a surface oil slick due to its interfacial

tension with water. Oil droplets form due to waves and wind (Moles et al. 2002). The submergence of oil droplets is enhanced by the application of dispersants which makes the droplets small. The size distribution of the oil droplets affects when these droplets resurface or remain dispersed in the water column (Boufadel et al. 2006, Boufadel et al. 2007, Chen and Yapa 2007). The interfacial area of oil droplets is also of utmost importance for oil dissolution and biodegradation (Vilcáez et al. 2013, Viveros-Thrift et al. 2015) Hence, estimation on the droplets size distribution is essential for quick and effective accidental oil spill response and contingency planning.

The complexity of physical and chemical interactions among oil, dispersants, and the seawater raises questions on how the use of dispersants, mixing energy and time impact the dispersion performance and droplets size distribution. Oil dispersants are complex mixtures of surfactants and solvents, which are frequently used after an oil spill to enable oil to mix with water more easily. Oil treated with dispersants is broken up into small droplets and get entrained into the water column when exposed to mixing energy (Kaku et al. 2006, Kaku et al. 2006, Li et al. 2008, Li et al. 2009, Li et al. 2009). Oil droplet dispersion is promoted by turbulence resulted from mixing energy imposed by waves (Delvigne 1993, Kaku et al. 2006). Additionally, mixing energy is one of the most important factors in determining the dispersion performance in the absence of dispersant, which is usually the case of natural dispersion. Relative to mixing energy, mixing time was reported to exert an insignificant effect on DE (Sorial et al. 2004). However, other researchers reported that mixing energy and time own statistically significant influences on DE (Mukherjee and Wrenn 2009).

To improve understanding of how and when to apply dispersants to minimize the negative impact of accidental oil spills, the effects of mixing energy and time on the dispersion performance and oil droplet size distribution with/without dispersant were systematically investigated in this work. The overall objective of this work was to compare the DE and droplet size distribution between two oils (Cold Lake Blend diluted bitumen, CLB and Alaska North Slope crude oil, ANS) without and with dispersants at different mixing energies and times.

2. Experiment

2.1 Synthetic seawater

Synthetic seawater (salinity 34 ppt) was prepared by dissolving 34 g of the commercially available Instant Ocean sea salt (Aquarium System of Mentor, Ohio, USA) in 1 L of ultrapure deionized water (Millipore, 18.2 MΩ*cm). The mixture was vigorously agitated using a magnetic stirrer. The seawater was filtered through 0.2 μm membrane filters (Millipore) to remove any suspended materials that might interfere with particle size measurements, and the solution was kept in the refrigerator at 15 ± 1 °C.

2.2 Baffled flask test

The EPA official standard protocol baffled flask test (BFT) was adopted to evaluate the dispersion effectiveness. The BFT protocol relies on using a 150-mL screw-cap trypsinizing flask with four baffles equally distributed on the side to allow for better mixing. The baffled flask was equipped with a glass stopcock near its bottom, so that a subsurface water sample could be collected without disturbing the surface oil layer.

The BFT protocol (Venosa and Holder 2013) is described as followings. A volume of 120 mL synthetic seawater was added to the baffled flask, followed by the addition of 100 μL of ANS or CLB using a 250-μL SGE™ gastight glass syringe with a steel luer lock tip. The oil was dispensed onto the center of the water surface gently. The exact mass of oil added was derived from the weight difference between the glass syringe with oil and that after dispensing the oil. Subsequently, 4 μL of Corexit 9500 (Nalco Energy Service, L.P. Sugar Land, TX) was added to the center of the oil slick in the baffled flask using a 1-10 μL Brinkmann Eppendorf repeater plus micropipette (Fisher Scientific, Pittsburgh, PA), giving the dispersant-to-oil volumetric ratio (DOR) of 1:25. The Corexit 9500 should be released as close as possible to the surface of the oil slick without actually touching it.

Following the addition of oil and dispersant, the flask was placed on the orbital shaker (Lab-Line Instruments Inc., Melrose Park, IL), with a variable speed control unit (40–400 rpm) and an orbital diameter of 2 cm, to provide designed mixing energy to the solutions in the test flasks. The experiments were performed in the Thermo Scientific Precision™ refrigerated incubator at 15 ± 1 °C. The rotation speeds selected in this work were 125 and 250 rpm. After each mixing time interval (5, 10, 60, and 120 min), the flask was removed from the shaker and kept stationary on the bench top for 10 min. Subsequently, the first 5 mL of sample was drained from the stopcock and discarded (Sorial et al. 2004, Sorial et al. 2004). Then, 40 mL of sample was collected into a 50 mL graduated cylinder. A subsample of 30 mL was used to measure oil concentration. Another 1 mL of subsample from the remaining 10 mL was used to measure the oil

droplet size distribution in the water column.

2.3 Oil standard procedure

For calibrating the Ultraviolet(UV)-Vis spectrophotometer, the oil stock solution was prepared by adding 2 mL of ANS or CLB measured using a 1-mL gas-tight syringe to 18 mL of dichloromethane (DCM, pesticide quality), and the concentration was then determined gravimetrically. Specific volumes (20, 50, 100, 150, 200, and 300 μL) of the oil stock solution were added to 30 mL of synthetic seawater in a 125-mL separatory funnel to generate 6-point calibration curve. Liquid-liquid extractions were performed (EPA 1996). The extraction procedure included (1) decanting the sample from the flask to a separatory funnel, (2) adding DCM and shaking vigorously for ~2 minutes, (3) allowing the DCM-oil and water phases to separate for ~5 minutes (the DCM is heavier than water and thus occupies the bottom of the separatory funnel), and (4) opening the stopcock and allowing the lower layer (DCM-oil phase) to drain into a clean glass beaker. Drain just to the point where the upper layer barely reaches the stopcock. The procedure was repeated until complete separation (DCM layer turned colorless). Subsequently, the extract was passed through column containing glass wool and anhydrous sodium sulfate to remove residual moisture, followed by adjusting the final extract to 30 mL using DCM. The samples were stored in 50-mL crimp style glass vials with aluminum/Teflon seals and mixed by inverting many times and then stored in a refrigerator at 4 °C until the time of analysis. The holding time was < 2 weeks.

For the dispersant-treated oil, an oil plus dispersant stock standard was first

prepared. The density of a stock solution consisting of 2 mL of specific reference oil, 80 μL of Corexit 9500, and 18 mL of DCM. The stock solution was used to prepare a 6-point oil standard calibration curve for treatments with dispersant as mentioned above.

The oil concentration was measured through the absorbance of the oil solution in DCM using a UV-VIS spectrophotometer (Cole Parmer 4802 Scanning Double Beam UV/Visible Spectrophotometer, IL, USA) at the wavelengths 340, 370, and 400 nm . The DCM was used as a blank solution initially, followed by the analysis of oil standards and samples. The absorbance was plotted against the wavelength and the area under the curve was calculated using the trapezoidal rule as following (Venosa and Holder 2013) :

$$\text{Area} = \frac{\left(\text{Abs}_{340} + \text{Abs}_{370}\right) \times 30}{2} + \frac{\left(\text{Abs}_{370} + \text{Abs}_{400}\right) \times 30}{2} \quad (1)$$

where, Abs_{340}, Abs_{370} and Abs_{400} are absorbance values at 340, 370, and 400 nm, respectively. The area in Eq. 1 was used to calculate the total oil dispersed in the water column following the equation:

$$\text{Total oil dispersed (g)} = \frac{\text{Area}}{\text{Calibration Curve Slope}} \times V_{\text{DCM}} \times \frac{V_{\text{tw}}}{V_{\text{ew}}} \quad (2)$$

DE is defined as the amount of total oil dispersed in the water column divided by the total amount of oil added (the percentage of oil dispersed) shown as follows:

$$\text{DE} = \frac{\text{Total oil dispersed}}{\text{m}_{\text{oil}}} \times 100 \quad (3)$$

where V_{DCM} is the volume of DCM extract; V_{tw} is the total volume of seawater in the baffled flask; V_{ew} is the total volume of seawater extracted; m_{oil} (g) is the mass of the

specific test oil added to test flask. The same calculations were made for the oil without dispersant.

2.5 Oil droplet size distribution

The oil droplet size distribution was measured using a LISST (Laser In-Situ Scattering and Transmissometry, LISST-100X, Type C, Sequoia Scientific, Seattle, WA) particle-size analyzer. The particle size distributions were subdivided into 32 particle size intervals located logarithmically from 2.5 to 461 μm in diameter. A volume of 1 mL sample was withdrawn from the stopcock of the baffled flask and diluted with 120 mL of DI water, and then poured carefully into the LISST chamber. The number concentration of the particles should be $<10^4$ mL^{-1} to prevent coincidence counting (Mukherjee and Wrenn 2011) thereby requiring a sample dilution factor of 100-5000 before measurement. The pipette tips were cut to enlarge the opening (≥2 mm) to minimize the effects of sample transfer on the droplet size distribution.

2.6 Interfacial tension (IFT) measurement

The instrument Grace M6500 Spinning Drop Tensiometer (Grace Instrument, Houston, Texas, USA) was used at room temperature to measure the IFT between oil and Ohmsett water. The glass capillary tube (2 mm ID, 95 mm long) was sequentially rinsed with DI water and artificial seawater before loading samples. A syringe with a needle containing ~0.25 mL of seawater and dispersant mixture was injected into the tube. Then, another syringe with a needle filled with oil was inserted into the already filled tube. The

oil was then pushed slowly to produce a droplet without generating any air bubbles. The needle was removed quickly in order not to leave any oil residue, and to get a pendant oil droplet. Subsequently, a Viton O-rings was inserted into grooves cut in the cylindrical Teflon plug's circumference, following which the Teflon plug was inserted snugly into the open end of the tube. The chamber then started rotating at selected speeds. When the droplet shape was steady, the diameter of the droplet and rotation speed was recorded for the calculation of IFT using Eq. 4:

$$\gamma = 1.44 \times 10^{-7} (\Delta P)(D^3)(\theta^2) \quad (4)$$

where, γ is the IFT in mN/m, ΔP is the density difference water and oil, expressed in g/mL, D is the diameter of the droplet in mm read directly from the instrument, and θ is rotation in rpm read directly from instrument.

3. Results

3.1 Dispersant Effectiveness

Figure 1 shows the DE of ANS crude oil without and with dispersant after 5, 10, 60, and 120 min of mixing at 125 and 250 rpm. Slight changes in DE as increasing time and mixing energy occurred for the cases without dispersant. DE in the absence of dispersant was a few orders of magnitude smaller than those with dispersant at the definite mixing energy and time. For example, DE at 125 rpm was 3.59% (Figure 1) without dispersant after 120 min of mixing, ~10-folds smaller than that (32.33%, Figure 1) with dispersant for the same mixing energy and time. This suggested the dominant role of dispersant in the increase of DE of ANS oil. Mixing energy and time exerted limited

impacts on the oil dispersion in the absence of chemical dispersant.

In the presence of dispersant, DE increased as increasing mixing energy and time. DE increased from 6.16% to 32.33% and from 39.17% to 55.29% after 5-120 min of mixing for the rotation speed of 125 rpm and 250 rpm, respectively. After 5 min of mixing, one noted that a significant increase in DE at 250 rpm (39.17%) than that at 125 rpm (6.16%). This indicated that mixing energy is a crucial element in enhancing the ANS oil dispersion. An early report concluded that the energy applied, energy dissipation or mixing energy may be the most important factor relating to dispersant effectiveness (Fingas and Banta 2008). In a real oil spill scenario, mixing energy is required to disperse large oil slick into small oil droplets following the application of dispersants. Increasing mixing energy produces smaller eddies formed from the energy dissipation, thus facilitating the breakup of oil droplets (Chandrasekar et al. 2005). The vigorous mixing imposed by waves is critical for successful application of dispersants (Boufadel et al. 2006, Kaku et al. 2006, Boufadel et al. 2007). Hence, DE is influenced by the ocean state. The rougher ocean state brings about better mixing of oil and dispersants, ultimately resulting in higher DE (Chandrasekar et al. 2005, Kaku et al. 2006).

Figure 2 reports the DE of CLB oil without and with dispersant after 5, 10, 60, and 120 min of mixing at 125 and 250 rpm. For the cases without dispersant, negligible DE of CLB was observed at 125 rpm. An increase in mixing energy (250 rpm) led to a limited elevation in DE of CLB. This indicated the inability of mixing energy to disperse CLB effectively without dispersant. Additionally, mixing time had a negligible effect on the DE of CLB in the absence of dispersant. Similar to DE of ANS crude oil, mixing

energy performed a significant function in the degree of DE in the presence of dispersant. Figure 2 shows that DE of CLB was greater at high mixing energy (250 rpm) than that at low mixing energy (125 rpm) with dispersant. In the presence of dispersant, DE of CLB was in a range of 0.87% to 3.59% at 125 rpm, while it spanned from 11.40% to 22.98% at 250 rpm. Thus, the results revealed that dispersibility of CLB was primarily governed by the addition of chemical dispersant. This reflected the fact that Corexit 9500 is designed to facilitate the formation of small droplets to improve the dispersibility of oil.

However, the degree of DE for CLB was several orders of magnitude smaller by comparison to that for ANS in the presence of dispersant, which may be ascribed to the different viscosity of two types of oil. CLB has a viscosity of 150 mPa·s at 15 °C (Environment Canada), more than 10-fold larger than that of ANS (13.11 mPa·s at 15 °C) (Fingas 2010), which makes the dispersant access the CLB oil slick with difficulty. Thus, it is possible that oil viscosity regulates how the dispersant behave in the oil/water interface, namely dispersant may not penetrate and mix well with CLB. This is in a close agreement with an earlier report that oil viscosity may determine mixing of dispersant into the oil slick. For more viscous oil, dispersant may be washed away before it mixes with the oil (Lee et al. 1981).

Note that the temporal changes in DE for CLB with dispersant were inconsistent, with a steady increase for the first 10 min of mixing, followed by a slight drop after 60 and 120 min of mixing at 250 rpm. DE of CLB continuously increased from 0.88% to 1.93% for the first 10 min of mixing, after which it dropped to 1.63% after 60 min of

shaking for the case with dispersant at 125 rpm. Unlike the ANS crude oil, mixing CLB and seawater for 120 min tended to prevent the CLB from continuous formation of small oil droplets from large oil slick, thereby reducing the extent of DE for CLB. This demonstrated that CLB droplets tended to recombine to resurface and reform surface slicks over time.

3.2 Oil droplet size distribution

3.2.1 ANS

Figure 3 reports the ANS oil droplet size distributions under different mixing time in the absence of dispersant for the low mixing speed of 125 rpm. In the absence of dispersant, the ANS exhibited fairly poor dispersion where the majority of the oil concentrated at or near the largest droplet size (~500 μm). Very limited oil was dispersed into the water column and its concentration was relatively small. After 2 h of mixing, the volume median diameter of the sample, d_{50} = 346.57 μm, is >50 orders of magnitude larger than that in the presence of dispersant under the same mixing speed, indicating that mixing for 2 h was insufficient for effective dispersion without the aid of dispersant. In addition, the absence of dispersant at 125 rpm generated d_{50} = 406.08, 180.82, 219.54, and 346.57 μm after 5, 10, 60, and 120 min of mixing, respectively. This suggested that the mixing time was unable to break up large ANS oil droplets into small ones without dispersant. The oil droplets produced by the mixing energy were typically larger than 100 μm and appeared to ascend and coalesce at the surface, reflected by the increase in d_{50} as increasing time. This may be due to the fact that physical dispersion is commonly

unstable and the destabilized physically dispersed oil droplets are inclined to coalescence to form large droplets. Large droplets will rise relatively quickly to the surface and reform the oil slick, while small droplets will rise more slowly and can be driven far away from the discharge location assisted with currents prior to getting to the surface (Johansen et al. 2013). The uniformly unimodal oil droplets size distribution was observed as limited effects of low mixing energy and mixing time in producing smaller oil droplets existed in the absence of chemical dispersant.

Figure 4 shows the ANS oil droplets size distribution in the absence of dispersant for the high rotation speed of 250 rpm. Unimodal, bimodal or multimodal droplet size distributions were observed for different mixing time. Similar to low mixing energy condition (rotation speed: 125 rpm), the absence of dispersant resulted in ineffective dispersion of crude oil in comparison with that in the presence of dispersant, indicating great importance of dispersant in promoting chemical dispersion. However, use of a high mixing energy (rotation speed: 250 rpm) without dispersant allowed more efficient dispersion, reflected by ~4-fold smaller values of d_{50} at 250 rpm than those at 125 rpm at the corresponding mixing time. Therefore, mixing energy became the most important factor in influencing the formation of smaller oil droplets for the case of physical dispersion.

Figure 5 shows ANS oil droplet size distributions over mixing time with the addition of dispersant at 125 rpm. Bimodal droplet size distribution was observed for the sample mixing for 5 min. The other samples mixing for 10 min ~ 2 h had a unimodal droplet size distribution. In the presence of dispersant, ANS crude oil was continuously

dispersed into the water column and large droplets were gradually broken up into small ones over time when mixing at 125 rpm, evidenced by the declining order of the characteristic droplet size, the volume median diameter d_{50} = 41.28, 151.57, 20.62, and 6.29 μm after 5, 10, 60, and 120 min of mixing, respectively. This indicated that the addition of dispersant steadily increased the amount of small oil droplets of ANS with increasing mixing time. Figure 5b shows that after 60 min of shaking, ~ 70% of droplets with < 70 μm was produced, while only ~30% of < 70 μm droplet size distribution was observed after 10 min of shaking. The findings were in a close agreement with earlier studies which have indicated that oil droplet sizes in the presence of dispersant under wave conditions span in the range of 2.5-70 μm in a unimodal, bimodal or multimodal droplet size distribution (Li et al. 2009, King et al. 2015).

Figure 6 reports the ANS oil droplets size distribution at different times using higher mixing energy (rotation speed: 250 rpm). In the presence of dispersant, increasing the mixing energy by two times resulted in faster formation of smaller droplets, reflecting very effective dispersion at higher mixing energy. After 5 min of shaking, more than 80% of droplets were < 3 μm. The amount of smaller droplets (< 10 μm) increased as increasing mixing time. The smallest droplets may remain dispersed in the water column for an extended time period by vertical oceanic turbulent (Johansen et al. 2013). In comparison with the oil dispersion at lower mixing energy, the significant increase in the production of small oil droplets in the water column at the corresponding time using higher mixing energy illustrated the importance of mixing energy in the dispersibility of crude oil in the presence of dispersant. This was in accordance with a previous study

stating that mixing energy is required to entrain small oil droplets into underlying water column with either a physical or chemical approach (Abdelrahim 2012). The oil and water interface becomes less stable after the use of dispersant and natural wind or wave turbulence aided by interfacial energy gradients will have a tendency to cause oil drops to shear from the slick (Mackay et al. 1984). Figure 4 shows smooth curves indicating that the chemically dispersed ANS oil droplets using higher mixing energy had a uniform and unimodal droplet size distribution and no propensity to ascend and coalesce at the surface to reform the oil slick.

3.2.2 CLB

Figure 7 shows the CLB droplet size distribution in the absence of dispersant at 125 rpm. Poor dispersion was observed due to the absence of dispersant. One notes a negligible change in the concentration of small CLB droplets after 5 and 10 min of mixing time. As the mixing time proceeded to 60 and 120 min, a slight increase in the smaller CLB droplets (< 200 μm) was noted, which indicate that mixing time had a certain but very limited effect on the CLB dispersion in the absence of dispersant. The undispersed CLB had a unimodal oil droplet size distribution shape after 5 and 10 min of mixing, while multimodal and broad droplet size distributions were observed after 60 and 120 min of mixing.

Figure 8 reports the CLB particle distribution in the absence of dispersant at 250 rpm. Similar to the case at 125 rpm, CLB at 250 rpm in the absence of dispersant remained undispersed and little CLB was driven into the water column; further indicating

that dispersant played a significant role in dispersing large oil droplets into small ones in the water column. This also suggested that the interface between CLB and water resisted deformation and remained relatively stable, even with the assistance of high mixing energy in the absence of dispersant. After 5, 10, and 60 min of mixing, CLB droplet particle distributions were uniformly unimodal with most CLB remained near the largest size (500 μm) that LISST can detect, while it changed to multimodal size distribution after 120 min of mixing.

Figure 9 reports CLB droplet distribution in the presence of dispersant at 125 rpm. Relative to ANS oil droplet distribution, CLB showed poorer dispersion under the same experimental condition, where >50% of oil droplets were larger than 150 μm, which may be due to the high viscosity characteristic of CLB. It is commonly recognized that heavy oil with high viscosity is not easily susceptible to chemical dispersion (Abdelrahim 2012). More than 90% of oil droplets were larger than 280 μm after 5 min of mixing, followed by a slight increase in the oil droplet of 10-75 μm after 10 min of mixing. The continuous mixing for 1 h provided a broad droplet size distribution with a remarkable appearance of smaller droplets (3-50 μm). However, after 2h of mixing, an appreciable portion of smaller droplets were absent while larger droplets (>400 μm) increased, which may be ascribed to that increasing mixing time tended to make the dispersed droplets ascend and coalesce at the surface. The droplet size distributions were unimodal, bimodal, multimodal, and unimodal after 5, 10, 60, and 120 min of mixing, respectively.

Figure 10 shows oil droplets size distribution with the addition of dispersant at

250 rpm. After 5 min of mixing, similar pattern of the distribution was observed for two different mixing speeds (125 and 250 rpm). However, an obvious discrepancy in the oil droplets size distribution was measured after 10 min and 60 min of mixing, where d_{50} values after 60 min of mixing were 150.29 and 38.29 μm for the mixing speed of 125 and 250 rpm, respectively. After 120 min of mixing, the similar tendency of coalescence was noted. The d_{50} value shifted from 38.29 μm after 60 min of mixing to 156.63 μm after 120 min of mixing. The dispersed CLB had unimodal oil droplet size distributions after 5 and 10 min of mixing, while multimodal droplet size distributions were observed for the samples after 60 and 120 min of mixing.

4. Discussion

The oil slick instability may be the primary mechanism for oil slick break-up into droplets. The instability depends mainly on surface forces, including interfacial tension, viscous forces, and hydrodynamic forces acting at the oil/water interface. As a consequence of these forces, the oil slick turns unable and is broken up into droplets (Chen and Yapa 2007). The occurrence of oil droplet breakup depends on whether the drag force acting on the droplets exceeds the interfacial tension or the local external turbulent energy surpasses the interfacial tension (Chen and Yapa 2007). A minimum amount of energy input is required when the interfacial tension between oil and water is reduced to permit the generation of oil droplets and a greater interfacial area (Abdelrahim 2012). The size of oil droplets resulted from either physical or chemical dispersion affects their following migration in the oil and water mixture. Larger size of oil droplets tend to move up quickly and reach the surface and reform the oil slick early, while

smaller size of oil droplets appear to transport far away from the initial spill locations and get entrained into the water column. This is confirmed by our finding in Figure 11 showing that chemical dispersion under high mixing energy generally gave greatest total droplets concentration (<500 μm) in the water column.

Viscosity of crude oil needs to be considered when chemical dispersant is in use due to the fact that viscosity is one of key factors controlling dispersant effectiveness (Canevari 1969, Martenelli and Lynch 1980, Stevens and Roberts 2003, Trudel et al. 2010). Date back to 1970s, one studies attributed the failure of dispersant use on the heavy fuel oil spills to limiting effects of oil viscosity on chemical dispersion of oil spills (Martenelli and Lynch 1980). Some researchers established the dispersant effectiveness versus oil viscosity relationship, with a declined dispersant effectiveness as increasing oil viscosity (Martinelli and Cormack 1979, Martenelli and Lynch 1980, Lee et al. 1981). Oil with low viscosity possesses weak resistance to deformation by shear stress; therefore dispersant addition reduces IFT between oil and water with ease, allowing oil to be sheared into small oil droplets and entrained into the water column with the aid of sufficient mixing energy (Lee et al. 1981, Trudel et al. 2010). In contrast, dispersant use hardly changes the resistance of high-viscosity oil to be sheared into small droplets, causing declined DE (Lee et al. 1981, Trudel et al. 2010). Coolbaugh et al. also reported that dispersants are not universally effective on all kinds of oil. Higher viscosity oils are less dispersible than low-viscosity oils (Coolbaugh et al.).

According to the rule "Like dissolves like", nonpolar oil and polar water, as two incompatible phases, are not attracted to each other. A chemical substance that is

miscible with both oil and water is needed to aid in the introduction of oil droplets into the water column. Corexit 9500, commonly used dispersant in real oil spill scenarios, contains the surfactant molecules with amphipathic characteristic. These surfactant molecules containing both hydrophobic and hydrophilic functional groups exhibit affinity for oil and water and serve as a seamless bridge between these two immiscible phases. Thus, the amphipathic characteristic of the surfactant molecules contained in the dispersant formulation will allow the dispersant to reside at the oil/water interface and tend to lower the interfacial tension between oil and water (Abdelrahim 2012), ultimately forming micron-sized oil droplets and driving them into the water column by energy input. Our visual observation of ANS oil specimens with/without dispersant further supported that the dispersant was very effective in dispersing oil slick into small oil droplets and entraining them into the water column (Figures 12a and 12c). On the contrary, the oil samples without dispersant resulted in relatively transparent water column and thick oil slicks floating on the surface (Figures 12b and 12d).

Figure 13 shows changes of IFT between oil and water over time in the presence of dispersant. Following the application of dispersant, IFT between ANS and water decreased steadily as a function of mixing time at both 125 and 250 rpm, with a higher degree of IFT reduction at 250 rpm, which is responsible for oil droplet distribution patterns and trend of DE of ANS under various experimental conditions. When IFT between oil and water gets lowered, cohesive forces of the oil film is weakened, resulting in facile entrainment of small oil droplets into the water column. This eventually enhances the oil dispersion, reflected by an increased DE of oil. However, the extent of

IFT reduction between CLB and water over time appeared to be limited and the IFT values decreased in the first 60 min of mixing, followed by a few percent of increase after 120 min of mixing. This is in parallel with the trends in CLB oil droplets distribution and DE of CLB under the same experimental conditions. The absence of smaller CLB droplets distributed in the water column and relatively smaller DE of CLB even in the presence of dispersant may be attributed to its resistance in IFT reduction as shown in Figure 13. Our findings were in accordance with previous studies reporting that the magnitude of reduction in oil/water IFT can be employed to assess the effectiveness of a chemical dispersant (Clayton et al. 1993, Abdelrahim 2012).

References

Abdelrahim, M. (2012). Measurement of interfacial tension in hydrocarbon/water/dispersant systems at deepwater conditions, Master Thesis, Louisiana State University.

Atlas, R. M. and T. C. Hazen (2011). "Oil biodegradation and bioremediation: a tale of the two worst spills in US history." Environ. Sci. Technol. **45**(16): 6709-6715.

Blondina, G. J., M. M. Singer, I. Lee, M. T. Ouano, M. Hodgins, R. S. Tjeerdema and M. L. Sowby (1999). "Influence of salinity on petroleum accommodation by dispersants." Spill Sci. Technol. B. **5**(2): 127-134.

Boufadel, M. C., A. Abdollahi-Nasab, X. Geng, J. Galt and J. Torlapati (2014). "Simulation of the Landfall of the Deepwater Horizon Oil on the Shorelines of the Gulf of Mexico." Environ. Sci. Technol. **48**(16): 9496-9505.

Boufadel, M. C., R. D. Bechtel and J. Weaver (2006). "The movement of oil under non-breaking waves." Mar. Pollut. Bull. **52**(9): 1056-1065.

Boufadel, M. C., K. Du, V. Kaku and J. Weaver (2007). "Lagrangian simulation of oil droplets transport due to regular waves." Environ. Modell. Softw. **22**(7): 978-986.

Boufadel, M. C., Y. Sharifi, B. Van Aken, B. A. Wrenn and K. Lee (2010). "Nutrient and Oxygen Concentrations within the Sediments of an Alaskan Beach Polluted with the Exxon Valdez Oil Spill." Environmental Science & Technology **44**(19): 7418-7424.

Brandvik, P. J. and P. S. Daling (1998). "Optimisation of oil spill dispersant composition by mixture design and response surface methods." Chemom. Intell. Lab. Syst. **42**(1): 63-72.

Canevari, G. P. (1969). General dispersant theory. International Oil Spill Conference, American Petroleum Institute.

Chandrasekar, S., G. A. Sorial and J. W. Weaver (2005). "Dispersant effectiveness on three oils under various simulated environmental conditions." Environ. Eng. Sci. **22**(3): 324-336.

Chen, F. and P. D. Yapa (2007). "Estimating the oil droplet size distributions in deepwater oil spills." J. Hydraul. Eng. .
Clayton, J. R., J. R. Payne, J. S. Farlow and C. Sarwar (1993). Oil spill dispersants: mechanisms of action and laboratory tests, Science Applications International Corp., San Diego, CA (United States).
Coolbaugh, T., A. McElroy and L. U. C. Guard Dispersant Efficacy and Effectiveness. Available from: http://crrc.unh.edu/sites/crrc.unh.edu/

files/coolbaughmcelroy.pdf.
Delvigne, G. A. (1993). Natural dispersion of oil by different sources of turbulence. International Oil Spill Conference, American Petroleum Institute.
Environment Canada, E. S. a. T. D. "Cold Lake Blend. Available from: http://www.etc-cte.ec.gc.ca/databases/Oilproperties/pdf/WEB_Cold_Lake_Blend.pdf."
EPA (1996). "Method 3510C: separatory funnel liquid-liquid extraction. Revison 3. pp.1-8.".
Fingas, M. (2010). "Review of the North Slope Oil properties relevant to environmental assessment and prediction." Spill Science, Edmonton, Alberta, Canada.
Fingas, M. and J. Banta (2008). A Review of Literature Related to Oil Spill Dispersants. Available from http://www.uscg.mil/iccopr/files/Lit_review_oil_spill_dispersants_PWSRCAC_.pdf.
Gong, Y., J. Fu, S. O'Reilly and D. Zhao (2015). "Effects of oil dispersants on photodegradation of pyrene in marine water." J. Hazard. Mater. **287**: 142-150.
Johansen, Ø., P. J. Brandvik and U. Farooq (2013). "Droplet breakup in subsea oil releases–Part 2: Predictions of droplet size distributions with and without injection of chemical dispersants." Mar. Pollut. Bull. **73**(1): 327-335.
Kaku, V. J., M. C. Boufadel and A. D. Venosa (2006). "Evaluation of mixing energy in laboratory flasks used for dispersant effectiveness testing." J. Environ. Eng. **132**(1): 93-101.
Kaku, V. J., M. C. Boufadel, A. D. Venosa and J. Weaver (2006). "Flow dynamics in eccentrically rotating flasks used for dispersant effectiveness testing." Environ. Fluid Mech. **6**(4): 385-406.
King, T. L., B. Robinson, C. McIntyre, P. Toole, S. Ryan, F. Saleh, M. C. Boufadel and K. Lee (2015). "Fate of Surface Spills of Cold Lake Blend Diluted Bitumen Treated with Dispersant and Mineral Fines in a Wave Tank." Environ. Eng. Sci. **32**(3): 250-261.
Kujawinski, E. B., M. C. Kido Soule, D. L. Valentine, A. K. Boysen, K. Longnecker and M. C. Redmond (2011). "Fate of dispersants associated with the Deepwater Horizon oil spill." Environ. Sci. Technol. **45**(4): 1298-1306.
Lee, M., F. Martinelli, B. Lynch and P. Morris (1981). The use of dispersants on viscous fuel oils and water in crude oil emulsions. International Oil Spill Conference, American Petroleum Institute.
Li, H. and M. C. Boufadel (2010). "Long-term persistence of oil from the Exxon Valdez spill in two-layer beaches." Nature Geoscience **3**(2): 96-99.
Li, Z., K. Lee, T. King, M. C. Boufadel and A. D. Venosa (2008). Oil droplet size distribution as a function of energy dissipation rate in an experimental wave tank. International Oil Spill Conference, American Petroleum Institute.
Li, Z., K. Lee, T. King, M. C. Boufadel and A. D. Venosa (2009). "Evaluating chemical dispersant efficacy in an experimental wave tank: 2—Significant factors determining in situ oil droplet size distribution." Environ. Eng. Sci. **26**(9): 1407-1418.
Li, Z., K. Lee, T. King, P. Kepkay, M. C. Boufadel and A. D. Venosa (2009). "Evaluating chemical dispersant efficacy in an experimental wave tank: 1, dispersant effectiveness as a function of energy dissipation rate." Environ. Eng. Sci. **26**(6): 1139-1148.
Mackay, D., A. Chau, K. Hossain and M. Bobra (1984). "Measurement and prediction of the

effectiveness of oil spill chemical dispersants." Oil Spill Chemical Dispersants, Research, Experience and Recommendations, ASTM STP **840**: 38-54.
Martenelli, F. and B. Lynch (1980). Factors affecting the efficiency of dispersants, Warren Spring Laboratory, Department of Industry.
Martinelli, F. and D. Cormack (1979). Investigation of the effects of oil viscosity and water-in-oil emulsion formation on dispersant efficiency, Warren Spring Lab., Stevenage (UK).
Moles, A., L. Holland and J. Short (2002). "Effectiveness in the laboratory of Corexit 9527 and 9500 in dispersing fresh, weathered, and emulsion of Alaska North Slope crude oil under subarctic conditions." Spill Sci.Technol. Bull. **7**(5): 241-247.
Mukherjee, B., J. Turner and B. A. Wrenn (2011). "Effect of oil composition on chemical dispersion of crude oil." Environ. Eng. Sci. **28**(7): 497-506.
Mukherjee, B. and B. A. Wrenn (2009). "Influence of dynamic mixing energy on dispersant performance: role of mixing systems." Environ. Eng. Sci. **26**(12): 1725-1737.
Mukherjee, B. and B. A. Wrenn (2011). "Effects of physical properties and dispersion conditions on the chemical dispersion of crude oil." Environ. Eng. Sci. **28**(4): 263-273.
Sorial, G. A., A. D. Venosa, K. M. Koran, E. Holder and D. W. King (2004). "Oil spill dispersant effectiveness protocol. I: Impact of operational variables." J. Environ. Eng. **130**(10): 1073-1084.
Sorial, G. A., A. D. Venosa, K. M. Koran, E. Holder and D. W. King (2004). "Oil spill dispersant effectiveness protocol. II: Performance of revised protocol." J. Environ. Eng. **130**(10): 1085-1093.
Stevens, L. and J. Roberts (2003). Dispersant effectiveness on heavy fuel oil and crude oil in New Zealand. International Oil Spill Conference, American Petroleum Institute.
Trudel, K., R. C. Belore, J. V. Mullin and A. Guarino (2010). "Oil viscosity limitation on dispersibility of crude oil under simulated at-sea conditions in a large wave tank." Mar. Pollut. Bull. **60**(9): 1606-1614.
Venosa, A. D. and E. L. Holder (2013). "Determining the dispersibility of South Louisiana crude oil by eight oil dispersant products listed on the NCP Product Schedule." Mar. Pollut. Bull. **66**(1): 73-77.
Vilcáez, J., L. Li and S. S. Hubbard (2013). "A new model for the biodegradation kinetics of oil droplets: application to the Deepwater Horizon oil spill in the Gulf of Mexico." Geochem. Trans **14**(4).
Viveros-Thrift, D., R. Jones and M. C. Boufadel (2015). The biodegradation model of the NOAA oil spill software ADIOS3. Arctic Marine Oil Spills, Vancouver, Canada, Environment Canada.
Wrenn, B., A. Virkus, B. Mukherjee and A. Venosa (2009). "Dispersibility of crude oil in fresh water." Environ. Pollut. **157**(6): 1807-1814.
Zhao, L., M. C. Boufadel, E. Adams, S. A. Socolofsky, T. King and K. Lee (2015). " Simulation of scenarios of oil droplet formation from the Deepwater Horizon blowout." Mar. Pollut. Bull. **In press**.
Zhao, L., M. C. Boufadel, S. A. Socolofsky, E. Adams, T. King and K. Lee (2014). "Evolution of droplets in subsea oil and gas blowouts: Development and validation of the numerical model VDROP-J." Mar. Pollut. Bull. **83**(1): 58-69.

To: chris.barker@noaa.gov[chris.barker@noaa.gov]; CJ.Beegle-Krause@sintef.no[CJ.Beegle-Krause@sintef.no]; Conmy, Robyn[Conmy.Robyn@epa.gov]; thomas.s.coolbaugh@exxonmobil.com[thomas.s.coolbaugh@exxonmobil.com]; fingasmerv@shaw.ca[fingasmerv@shaw.ca]; ali.khelifa@ec.gc.ca[ali.khelifa@ec.gc.ca]; jrpayne@sbcglobal.net[jrpayne@sbcglobal.net]; wspegau@pwssc.org[wspegau@pwssc.org]; creddy@whoi.edu[creddy@whoi.edu]
Cc: nancy.kinner@unh.edu[nancy.kinner@unh.edu]
From: Mandsager, Kathy
Sent: Tue 5/17/2016 6:51:30 PM
Subject: RE: State-of-Science for Dispersants: Physical Transport & Chemical Behavior
references from public input.docx

Please find attached a list of references collected from the public input submissions. They are in no particular order.

It will take us a little while to collect these manuscripts and include them in the database if that is indeed the next step.

From: Mandsager, Kathy
Sent: Friday, April 22, 2016 2:30 PM
To: 'chris.barker@noaa.gov' <chris.barker@noaa.gov>; 'CJ.Beegle-Krause@sintef.no' <CJ.Beegle-Krause@sintef.no>; 'conmy.robyn@epa.gov' <conmy.robyn@epa.gov>; 'thomas.s.coolbaugh@exxonmobil.com' <thomas.s.coolbaugh@exxonmobil.com>; 'fingasmerv@shaw.ca' <fingasmerv@shaw.ca>; 'ali.khelifa@ec.gc.ca' <ali.khelifa@ec.gc.ca>; 'jrpayne@sbcglobal.net' <jrpayne@sbcglobal.net>; 'wspegau@pwssc.org' <wspegau@pwssc.org>; 'creddy@whoi.edu' <creddy@whoi.edu>
Cc: Kinner, Nancy <Nancy.Kinner@unh.edu>
Subject: RE: State-of-Science for Dispersants: Physical Transport & Chemical Behavior

Please mark your calendar for our next meeting on **Tuesday 17 May** at 2 – 4 pm ET via WebEx

(I will also send this to you in outlook calendar request for your convenience.)

WebEx login instructions:

Meeting number:

737 338 651

Meeting link: https://crrc.webex.com/crrc/j.php?MTID=m896ccec646ea639cc38bd4b8243bbd44

Audio connection:

1-855-244-8681 Call-in toll-free number (US/Canada)

1-650-479-3207 Call-in toll number (US/Canada)

Global call-in numbers

Show toll-free dialing restrictions

Access code: 737 338 651

From: Mandsager, Kathy
Sent: Tuesday, April 19, 2016 11:48 AM
To: 'chris.barker@noaa.gov' <chris.barker@noaa.gov>; 'CJ.Beegle-Krause@sintef.no' <CJ.Beegle-Krause@sintef.no>; 'conmy.robyn@epa.gov' <conmy.robyn@epa.gov>; 'thomas.s.coolbaugh@exxonmobil.com' <thomas.s.coolbaugh@exxonmobil.com>; 'fingasmerv@shaw.ca' <fingasmerv@shaw.ca>; 'ali.khelifa@ec.gc.ca' <ali.khelifa@ec.gc.ca>; 'jrpayne@sbcglobal.net' <jrpayne@sbcglobal.net>; 'wspegau@pwssc.org' <wspegau@pwssc.org>; 'creddy@whoi.edu' <creddy@whoi.edu>
Cc: Kinner, Nancy <Nancy.Kinner@unh.edu>
Subject: State-of-Science for Dispersants: Physical Transport & Chemical Behavior

Dear scientific panel:

The public input period has closed on the *Physical Transport & Chemical Behavior* document. We received 10 individual responses. A collated list of these responses are attached for your perusal.

It is now time to schedule another WebEx meeting in order to discuss this information and/or incorporate or edit the original document as you deem appropriate. Please use the doodle poll to select a time for this WebEx meeting in May. It is time-zone enabled for your convenience and if you could **respond by Monday 4/25** it will help in securing a date and getting it on your busy calendars.

Here is the doodle poll>> http://doodle.com/poll/8wn9ez5xpmeyhw2p

Thank you so much!

Kathy Mandsager

Coastal Response Research Center

Center for Spills and Environmental Hazards

220 Gregg Hall, 35 Colovos Rd

University of New Hampshire

Durham, NH 03824

603.862.1545

Afenyo, M., B. Veitch, and F. Khan, 2015. A state of the art review of fate and transport of oil spills in open and ice covered waters, Ocean Engineering, http://dx.doi.org/10.1016/j.oceaneng.2015.10.014.

Beegle-Krause, C.J., Simmons, H., McPhee, M., Daae, R.L., Reed, M., 2013. Fate of dispersed oil under ice Final Report 1.4 Literature Review, Arctic Oil Spill Response Technology Joint Industry Programme (JIP) p. 48.

Brandvik, P.J. and Faksness, L. G., 2009. Weathering processes in Arctic oil spills: Meso-scale experiments with different ice conditions. Cold Regions Science and Technology, 55(1): 160-166.

Emergency Prevention, Preparedness, and Response (EPPR), 2015. Guide to oil spill response in snow and ice conditions in the Arctic, EPPR Arctic Council.

Faksness, L. G., Brandvik, P.J., Daae, R.L., Leirvik, F. and Børseth, J.F., 2011. Large-scale oil-in-ice experiment in the Barents Sea: Monitoring of oil in water and MetOcean interactions. Marine Pollution Bulletin, 62(5): 976-984.

French McCay, D., Gearon, M.S., Kim, Y.H., Jayko, K. and Isaji, T., 2014. Modeling oil transport and fate in the Beaufort Sea. pp 40-64. In proceedings of the 37th Arctic and Marine Oilspill Program Technical Seminar. Environment Canada. Ottawa, ON. Canada.

Lewis, A., 2013. Arctic Oil Spill Response Technology Joint Industry Programme (JIP): Dispersant testing under realistic conditions. FINAL REPORT 2.1: Report from Joint Industry Programme to identify and summarise the state-of-the-art on research conducted to date on the effectiveness of dispersant and mineral fines in ice Available online: http://www.arcticresponsetechnology.org/wp-content/uploads/2013/10/Report 2.1 - DISPERSANT TESTING UNDER REALISTIC CONDITIONS.pdf.

Khelifa, A., Charron, D. M., Tong, T.-S., Singh, N. R., 2011. Effects of chemical dispersants on oil-brine interfacial tension and droplet formation: New results using new high resolution imaging setup and weathed oils. In: Proceedings of the 34th Arctic and Marine OilSpill Program Technical Seminar, Environment Canada, Ottawa, Canada, pp. 865-879.

Venkataraman, P., Tang, J., Frenkel, E., McPherson, G.L., He, J., Raghavan, S.R., Kolesnichenko, V.L., Bose, A., John, V.T., 2013. Attachment of a Hydrophobically Modified Biopolymer at the Oil-Water Interface in the Treatment of Oil Spills. Applied Materials and Interfaces 5: 3572-3580.

Spaulding, M.L., Mendelsohn, D., Crowley, D., Li, Z. and Bird, A., 2015. Draft Technical Reports

for Deepwater Horizon Water Column Injury Assessment: Application of OILMAP DEEP to the Deepwater Horizon Blowout. September 30, 2015; Project No, 2011-144. RPS ASA, 55 Village Square Drive, South Kingstown, RI 02879. DWH-AR0285366. See Appendix G, Development of OILMAP DEEP droplet size model.

French McCay, D., Jayko, K., Li, Z., Horn, M., Kim, Y., Isaji, T., Crowley, D., Spaulding, M., Fontenault, J., Shmookler, R. and Rowe, J., 2015. Technical Reports for Deepwater Horizon Water Column Injury Assessment WC_TR.14: Modeling Oil Fate and Exposure Concentrations in the Deepwater Plume and Rising Oil Resulting from the Deepwater Horizon Oil Spill; Date of Report: September 29, 2015. Project No, 2011-144. RPS ASA, 55 Village Square Drive, South Kingstown, RI 02879. DWH-AR0285776.

Zhao, L., Boufadel, M. C., Socolofsky, S. A., Adams, E., King, T., Lee, K., 2014. Evolution of droplets in subsea oil and gas blowouts: Development and validation of the numerical model VDROP-J. Marine Pollution Bulletin 83:58-69.

Zhao, L., Boufadel, M.C., Adams, E., Socolofsky, S.A., King, T., Lee, K. and Nedwed, T., 2015. Simulation of scenarios of oil droplet formation from the Deepwater Horizon blowout. Marine Pollution Bulletin, 101: 304-319.

Spaulding, M.L., Mendelsohn, D., Crowley, D., Li, Z. and Bird, A., 2015. Draft Technical Reports for Deepwater Horizon Water Column Injury Assessment: Application of OILMAP DEEP to the Deepwater Horizon Blowout. September 30, 2015; Project No, 2011-144. RPS ASA, 55 Village Square Drive, South Kingstown, RI 02879. DWH-AR0285366.

Le Floch, S., S. Van Ganse, R. Mauge, and A. Laurent. 2013. Influence of Dispersant Addition on the Rise of Oil Droplets Contribution to Modelling. Proceedings of the thirty-Sixth Arctic and Marine Oil spill Program (AMOP) Technical Seminar on Environmental Contamination and Response, Environment Canada, Ottawa, Ontario, p. 315-325.

Spill Name: Saraband / **Location:** Canada / **Year:** 1998 / **Reference:** Rivet, Claude, 2000. Oil in Ice: The St. Lawrence Experience. Proceedings of the 2000 International Oil & Ice Workshop, Alaska Clean Seas, Prudhoe Bay, AK.

Brandvik, P.J., L-G. Faskness. 2009. Weathering Processes in Arctic Oil Spills: Meso-scale Experiments with Different Ice Conditions. Cold Regions Science and Tech nology, 55, 160□166.

EPPR, 2015, Guide to oil spill response in snow and ice conditions. Emergency Prevention, Preparedness and Response (EPPR). ISBN 978-82-999755-7-5. p 184

Brandvik, P.J., L.G. Faksness, P. Daling and I. Singsaas (2005). "Fate and behavior of oil spills under Arctic conditions. Earlier results compared with new field experiments on Svalbard".

AMAP International Symposium on Oil and Gas Activities in the Arctic i St.Petersburg, 13.-15. September, 2005, pp. 584-590.

Brandvik, P.J., Singsaas, I. and Daling, P.S. 2004: Oil Spill R&D in Norwegian Arctic Waters with Special focus on Large-Scale Oil Weathering Experiments. In proceedings from the Interspill 2004 conference, Trondheim Norway.

Cormack, D. and J. A. Nichols. 1977. The concentrations of oil in sea water resulting from natural and chemically induced dispersion of oil slicks. Proceedings of the 1977 International Oil Spill Conference, Washington DC, American Petroleum Institute, pp. 381-385.

Daling, P. S. and G. Indrebo. 1996. Recent improvements in optimizing use of dispersants as a cost-effective oil spill countermeasure technique. International Conference on Health, Safety & Environment, New Orleans, 9-12 June 1996.

Dickins 2003. Behavior of Oil Spills in Ice and Implications for Arctic Spill Response. In Proceedings of OTC Arctic Technology Conference, 7-9 February, Houston, Texas, USA.

Dickins, 1992. Behaviour of oil spilled at sea (BOSS). http://www.bsee.gov/Technology-and-Research/Oil-Spill-Response-Research/Reports/100-199/120At/

El-Tahan, H. And S. Venkatesh, 1994: Behavior Of Oil Spills In Cold And Ice-Infested Waters – Analysis Of Experimental Data On Oil Spreading. Proceedings Of The 17th Arctic And Marine Oil Spill Program (AMOP) Technical Seminar. Environment Canada, Pp. 337 - 354.

Fingas, M.F. and B.P. Hollebone, 2003: Review of behaviour of oil in freezing environments. Marine Pollution Bulletin, Vol. 47, pp. 333-340.

Fingas, M.F., B.P. Hollebone (2002). Behaviour of Oil in Freezing Environments: A Literature Review. In Proceedings of the 25th Artic and Marine Oilspill Program (AMOP) Technical Seminar, volume 2, pp. 1191-1205.

French McCay, D. P. and J. R. Payne. 2001. Model of oil fate and water concentrations with and without application of dispersants. Proceedings of the 24th Arctic and Marine Oil Spill Program (AMOP) Technical Seminar. Environment Canada, Ottawa, Canada, pp. 611-645.

French McCay, D. P., J. J. Rowe, W. Nordhausen, and J. R. Payne. 2006. Modeling potential impacts of effective dispersant use on aquatic biota. Proceedings of the 29th Arctic and Marine Oil Spill Program (AMOP) Technical Seminar. Environment Canada, Ottawa, Canada, pp. 855-878.

Hazen, T. C., E. A. Dubinsky, T. Z. DeSantis, G. L. Andersen, Y. M. Piceno, N. Singh, J. R. Jansson, A. Probst, S. E. Borglin, J. L. Fortney, W. T. Stringfellow, M. Bill, M. S. Conrad, L. M. Tom, K. L. Chavarria, T. R. Alusi, R. Lamendella, D. C. Joyner, C. Spier, M. Auer, M. L. Zemla, R. Chakraborty, E. L. Sonnenthal, P. D'haeseleer, H.-Y. N. Holman, S. Osman, Z. Lu, J. D. Van Nostrand, Y. Deng, J. Zhou, and O. U. Mason. "Deep-sea oil plume enriches psychrophilic oil-degrading bacteria". *Science* 330:204-208, 2010.

Lee, K., Nedwed, T., Prince, R. C., & Palandro, D., 2013 "Lab tests on the biodegradation of chemically dispersed oil should consider the rapid dilution that occurs at sea." Marine pollution bulletin, 73(1), 314-318.

McAuliffe, C., R. Steelman, W. Leek, D. Fitzgerald, and J. Ray. 1981. 1979 Southern California dispersant treated research oil spills. Proceedings of the 1981 International Oil Spill Conference, Washington, DC, American Petroleum Institute, pp. 269–282.

McAuliffe, C. D., J. C. Johnson, S. H. Greene, G. P. Canevari, and T. D. Searl. 1980. Dispersion and weathering of chemically treated crude oils on the ocean. Environmental Science & Technology, 14(12): 1509-1518.

Lunel, T. 1994. Dispersion of a large experimental slick by aerial application of dispersant. Arctic and Marine Oil Spill Program Technical Seminar. Proceedings of the Seventeenth Arctic and Marine Oilspill Program (AMOP) Technical Seminar, Vancouver, British Columbia, Canada, pp 951–979.

MMS, 2003. Persistence Of Crude Oil Spills On Open Water Project Number 1435-01-02-RP-85091 http://www.boem.gov/BOEM-Newsroom/Library/Publications/2003/2003-047.aspx

National Academies 2003. Oil in the Sea III: Inputs, Fates, and Effects. ISBN 0-309-08438-5

Strom-Kristiansen, T., J. Hokstad, A. Lewis, P. J. Brandvik. 1997. NOFO 1996—Oil on water exercise: Analysis of sample material. STF66 A97050. SINTEF, Trondheim, Norway.

Trudel, K., R. Belore, M. VanHaverbeke, and J. Mullin. 2009. Updating the U.S. SMART dispersant efficacy monitoring protocol. Proceedings of the Arctic and Marine Oilspill Program (AMOP) Technical Seminar, Environment Canada, Ottawa, Canada, pp. 397-410.

Horner-Devine, A.R., R. D. Hetland, and D. G. MacDonald, 2015. Mixing and Transport in Coastal River Plumes. *Annual Review of Fluid Mechanics* **47**, 569-594.

McClelland, J. W., A. Townsend-Small, R. M. Holmes, F. Pan, M. Stieglitz, M. Khosh, and B. J. Peterson (2014), River export of nutrients and organic matter from the North Slope of Alaska to the Beaufort Sea, *Water Resour. Res.*, 50, 1823–1839, doi:10.1002/2013WR014722.

Nghiem, S. V., D. K. Hall, I. G. Rigor, P. Li, and G. Neumann, 2014, Effects of Mackenzie River discharge and bathymetry on sea ice in the Beaufort Sea, *Geophys. Res. Lett.*, 41, 873–879, doi:10.1002/2013GL058956.

Kleindienst et al., PNAS | December 1, 2015 | vol. 112 | no. 48, pp. 14900–14905. *Chemical dispersants can suppress the activity of natural oil-degrading microorganisms*.

AEA Technology. 1994. International calibration of laboratory dispersant test methods against sea trials. Oxfordshire, UK: AEA Technology.

AEA Technology. 1995. International calibration of laboratory dispersant test methods against sea trials. Field trial report. July 1995 sea trials. Oxfordshire, UK: AEA Technology.

Baelum, J. Borglin S., Chakraborty R., Fortney J.L., Lamendella R., Mason O.U., Auer M., Zemla M., Bill M., Conrad M.E., Malfatti S.A., Tringe S.G., Holman H.-Y., Hazen T.C., Jansson J.K. 2012. Deep-sea bacteria enriched by oil and dispersant from the Deepwater Horizon spill. Environ Microbiol. Vol 14(9):2405-16. Retrived from doi: 10.1111/j.1462-2920.

Brandvik, Per Johan, Per Snorre Daling, Live-Guri Faksness, Janne Fritt-Rasmussen, Ragnhild Lundmark Daae, and Forde Leirvik. Experimental Oil Release in Broken Ice-A Large-Scale Field Verification of Results From Laboratory Studies of Oil Weathering and Ignitability of Weathered Oil Spills. Report no.: 26. SINTEF, 20 Apr. 2010. Web. 18 Feb. 2016.

Daling, Per, Arne Holumsnes, Claus Rasmussen, Per Johan Brandvik, and Frode Leirvik. Development and Testing of Containerized dispersant Spray System Use in Cold and Ice-Covered Waters. Rep. no. 13. N.p.: SINTEF, 2010. Print. JIP Oil in Ice.

Coelho, G., D. Aurand, L. Essex, A. Parkin, and L. Robinson. 2012. Monitoring subsurface dispersant injection during the MC252 incident, Volume 1. Lusby, MD, USA: Ecosystem Management & Associates, Inc.

Hazen, T., E. Dubinsky, T. DeSantis, G. Andersen, Y. Piceno, N. Singh, J. Jansson, A.Probst, S. Borglin, J. Fortney, W. Stringfellow, M. Bill, M. Conrad, L. Tom, K. Chavarria, T. Alusi, R. Lamendella, D. Joyner, C. Spier, J. Baelum, M. Auer, M. Zemla, R. Chakraborty, E. Sonnenthal, P. D'haeseleer, H-Y Holman, S. Osman, Z. Lu, J. Van Nostrand, Y. Deng, J. Zhou, O. Mason. 2010. Deep-Sea Oil Plume Enriches Indigenous Oil-Degrading Bacteria. Science Vol 330 (6001), pp. 204-208. Retrieved from doi: 10.1126/science.1195979

Jones, M., & Petch, S. (1995). A report on the analysis of hydrocarbons in sea waters and associated samples from trial oil spills off eastern England, July 1995. Newcastle upon Tyne, UK: University of Newcastle upon Tyne.

Operational Science Advisory Team (OSAT 1). (2010). Summary Report for Sub-sea and Sub-surface Oil and Dispersant Detection: Sampling and Monitoring. Unified Area Command, New Orleans. Retrieved from: http://www.dep.state.fl.us/deepwaterhorizon/files2/osat_report_17dec.pdf.

Prince, R. K. McFarlin, J. Butlera, E. Febbo, F. Wang, and T. Nedwed. 2013. The primary biodegradation of dispersed crude oil in the sea. Chemosphere Vol 90(2), pp. 521–526.

SL Ross Environmental Research & MAR Incorporated. (2007). Corexit 9500 Dispersant Effectiveness Testing in Cold Water on Four Alaskan Crude Oils. Herndon, VA: Minerals Management Service.

SL Ross Environmental Research Ltd. 2015. Tests to Evaluate the Effectiveness of Accel-DWD Dispersant on Louisiana Light Sweet Crude Oil. Ottawa, Ontario. 13 pp + appendices.

Steffek. 2015. Comparative Testing of Corexit EC9500A, Finasol OSR52, Accell Clean DWD, and ZI 400 at Ohmsett in a Simulated Arctic Environment. Interspill Conference, Amsterdam. 8 pp. Retrieved from: http://www.ohmsett.com/scientific/Comparative%20Testing%20of%20Corexit%20EC9500A,%20Finasol%20OSR52,%20Accell%20Clean%20DWD,%20and%20ZI%20400...%20-%20T%20Steffek,%20BSEE.pdf

Strøm-Kristiansen, T., Hokstad, J.N., Lewis, A., and Brandvik, P.J. (1997). NOFO 1996 oil on water exercise – analysis of sample material. SINTEF Data report number STF66 A97050. Trondheim, Norway.

Field Techniques for Sea Ice Research. 2009. Edited: Eicken, Hajo, Gradinger, Rolf, Salganek, Maya, Shirasawa, Kunio, Perovich, Don, and Leppäranta, Matti.
This reference is particular helpful in discussing data gaps of mathematical models.

Hutchings, JF, Petrich, C, Lindsay, R, Roberts, A, Zhang, J. 2009. "The Use of Models in the Design and Interpretation of Field Measurements" p. 483 in Field Techniques for Sea Ice Research. Edited: Eicken, Hajo, Gradinger, Rolf, Salganek, Maya, Shirasawa, Kunio, Perovich, Don, and Leppäranta, Matti.

Burke, J. 2011. "What's the difference between a hurricane and Alaska's mega storm?" Alaska Dispatch News, Nov. 9, 2011. Available at http://www.adn.com/article/whats-difference-between-hurricane-and-alaskas-mega-storm (last visited March 11, 2016).

Oliver, S.G. 2016. "'One storm away from a catastrophe,' Barrow seeks money for seawall". Arctic Sounder, Feb. 29, 2016. Available at http://www.adn.com/article/20160229/one-storm-away-catastrophe-barrow-seeks-money-seawall (last visited March 11, 2016).

Rosen, Y. 2015. "High winds cause flooding in Barrow, prompt Shell to pause oil drilling" Alaska Dispatch News. Aug. 27, 2015. Available at http://www.adn.com/article/20150827/high-winds-cause-flooding-barrow-prompt-shell-pause-oil-drilling (last visited March 11, 2016).

University of Alaska Fairbanks and BOEM, Chukchi and Western Beaufort Circulation Studies. http://dm.sfos.uaf.edu/chukchi-beaufort/ (last visited March 11, 2016).

Leandra de Sousa, Ph.D., Todd Sformo, Ph.D. North Slope Borough, Department of Wildlife Management. Satellite-tracked Surface Drifter Measurements off Barrow and Wainwright, Alaska, http://www.north-slope.org/departments/wildlife-management/studies-and-research-projects/oceanography-and-sea-ice/oceanography-and-sea-ice-research#OceanDriftersProject

(last visited March 11, 2016).

http://www.adn.com/article/20150827/high-winds-cause-flooding-barrow-prompt-shell-pause-oil-drilling (last visited March 11, 2016).

University of Alaska Fairbanks and BOEM, Chukchi and Western Beaufort Circulation Studies. http://dm.sfos.uaf.edu/chukchi-beaufort/ (last visited March 11, 2016).

Leandra de Sousa, Ph.D., Todd Sformo, Ph.D. North Slope Borough, Department of Wildlife Management. Satellite-tracked Surface Drifter Measurements off Barrow and Wainwright, Alaska, http://www.north-slope.org/departments/wildlife-management/studies-and-research-projects/oceanography-and-sea-ice/oceanography-and-sea-ice-research#OceanDriftersProject (last visited March 11, 2016)

To: Venkatapathy, Raghuraman[Venkatapathy.Raghuraman@epa.gov]
Cc: Conmy, Robyn[Conmy.Robyn@epa.gov]; Schubauer-Berigan, Joseph[Schubauer-Berigan.Joseph@epa.gov]
From: McClellan, Kim
Sent: Wed 9/16/2015 9:55:54 PM
Subject: Clearance of Abstracts
Solidifier_Abstract 2016 GOMRI_final.docx
ABSTRACT for Biodegradability of Dispersed Heavy Fuel Oil at 5 and 25 C_final.docx

Hi Raghu,

Complete Citation and Review	Brian Dyson	Devi Sundaravadivel	ORD-012921	Evaluation of Sorbent and Solidifier Properties and their Impact on Oil Removal Efficiency	Abstract	9/16/2015 4:47 PM
Complete Citation and Review	Brian Dyson	Mobing Zhuang	ORD-013917	Biodegradability of Dispersed Heavy Fuel Oil at 5 and 25 C	Abstract	9/16/2015 4:46 PM
Complete Citation and Review	Brian Dyson	Ruta Deshpande	ORD-013912	Biodegradability Of Diluted Bitumen Oil By Kalamazoo River Cultures In Freshwater	Abstract	9/16/2015 4:31 PM

These three abstracts have been cleared through STICS. The abstracts (ORD-012921, and ORD-013917) were changed by Alice Gilliland, LRPCD's Acting Division Director, and I will include them as attached files above.

I am still waiting on the clearance for "Biodegradation of Finasol OSR 52 and Dispersed Alaska North Slope Crude Oil at 5 C and 25 C" (ORD-013915). As soon as I receive the completion of the clearance, I will contact you via an email.

Thanks,

Kim

ABSTRACT

Biodegradability of Dispersed Heavy Fuel Oil at 5 and 25 C

Mobing Zhuang, Gulizhaer Abulikemu, Pablo Campo, Makram Suidan, Albert Venosa, and Robyn Conmy

2016 Gulf of Mexico Oil Spill & Ecosystem Science Conference

Fuel oil is produced by blending heavy residual oils with a lighter oil to meet specifications for viscosity and pour point. Compared to lighter oils, the high density and viscosity of fuel oil make it less susceptible to dispersion and biodegradation. Hence, heavy fuel oil spills could cause more serious damage to the environment and be more difficult to clean. The environmental impacts include coating of wildlife that dwell on the water surface, depleting oxygen in the receiving environment, exposing aquatic species to toxic substances, and sediment contamination. Laboratory experiments were conducted to study the biodegradability of Intermediate Fuel Oil 120 (IFO-120) dispersed by Corexit 9500 (C9500) at 5 and 25 °C. The biodegradability of alkanes and aromatics in IFO-120 at both temperatures was studied in the presence and absence of dispersant. When compared with IFO-120 alone treatments, data indicated that the depletion rate of alkanes at both temperatures was unaffected by the presence of dispersant. Conversely, C9500 significantly improved the uptake of aromatics as its presence shortened the lag phase at 25 °C from 4 to 2 days and increased their removal extent from 71 to 82%. At 5 °C, the addition of C9500 also improved the overall removal from 70 to 85%. Such enhancement effect could be explained by the promotion of dissolution of soluble aromatics in the presence of surfactants.

To: Conmy, Robyn[Conmy.Robyn@epa.gov]
From: Mike Fulton - NOAA Federal
Sent: Tue 5/17/2016 3:32:11 PM
Subject: Re: purchase fo finasol and corexit

Hi Robyn,
Have you heard that samples from DWH are going to be released? I believe they have Corexit 9500.
Mike

On Tue, Apr 12, 2016 at 12:59 PM, Mike Fulton - NOAA Federal <mike.fulton@noaa.gov> wrote:

> Good luck. You may have more leverage than we did. At one point, I thought we were very close to getting some, but their attorneys changed their mind.
>
> On Tue, Apr 12, 2016 at 8:56 AM, Conmy, Robyn <Conmy.Robyn@epa.gov> wrote:
>
> > Thanks Mike. This is our same contact, so I guess I will just keep trying to reach her. EPA is looking to procure a few gallons and will be doing toxicity testing. We will ask nicely and point out that the testing will be used to help with finalizing the NCP Subpart J language. If they still won't sell, we will look into if there is regulatory language that exists to help convince them to waive the waiver requirements. As you know, access to Nalco dispersants is quite a challenge for research.
> >
> > Cheers,
> >
> > Robyn
> >
> > <>/<>/<>/<>/<>/<>/<>/<>/<>/<>/<>/<>/<>/<>/<>/<>/<>/<>/<>/<>
> >
> > Robyn N. Conmy, Ph.D.
> >
> > Research Ecologist
> >
> > USEPA/NRMRL/LRPCD
> >
> > 26 West MLK Drive
> >
> > Cincinnati, Ohio 45268
> >
> > 513-569-7090 (office)
> >
> > 513-431-1970 (EPA mobile)
> >
> > 727-692-5333 (Personal mobile)

conmy.robyn@epa.gov

From: Mike Fulton - NOAA Federal [mailto:mike.fulton@noaa.gov]
Sent: Tuesday, April 12, 2016 8:41 AM

To: Conmy, Robyn <Conmy.Robyn@epa.gov>
Subject: Re: purchase fo finasol and corexit

Hi Robyn,

See below contact info for NALCO. You may have more success if you can sign a waiver that you won't use for toxicity testing. Good luck.

Mike

Debby.Theriot@nalco.com

281 263 7709

On Tue, Apr 12, 2016 at 7:58 AM, Conmy, Robyn <Conmy.Robyn@epa.gov> wrote:

> Thanks Mike. I spoke to a contact at Total yesterday and we are getting some Finasol. Nalco hasn't responded to a voicemail as of yet, so your contact at Nalco could be a huge help.
>
> <>/<>/<>/<>/<>/<>/<>/<>/<>/<>/<>/<>/<>/<>/<>/<>/<>/<>/<>
>
> Robyn N. Conmy, Ph.D.
>
> Research Ecologist
>
> USEPA/NRMRL/LRPCD
>
> 26 West MLK Drive

Cincinnati, Ohio 45268

513-569-7090 (office)

513-431-1970 (EPA mobile)

727-692-5333 (Personal mobile)

conmy.robyn@epa.gov

From: Mike Fulton - NOAA Federal [mailto:mike.fulton@noaa.gov]
Sent: Monday, April 11, 2016 5:00 PM
To: Conmy, Robyn <Conmy.Robyn@epa.gov>
Subject: Re: purchase fo finasol and corexit

Hi Robyn, Ultimately, We weren't able to get Corexit from Nalco, but I'll get you the contact info for both manufacturers.

On Monday, April 11, 2016, Conmy, Robyn <Conmy.Robyn@epa.gov> wrote:

> Hi Mike,
>
> Awhile back we had discussed NOAA's possible procurement of Corexit and Finasol for your toxicity work. Would you mind sharing the POC for Nalco and Total that were contacted in your hunt to procure the dispersants?
>
> Thanks,
>
> Robyn

<>/<>/<>/<>/<>/<>/<>/<>/<>/<>/<>/<>/<>/<>/<>/<>/<>/<>

Robyn N. Conmy, Ph.D.

Research Ecologist

USEPA/NRMRL/LRPCD

26 West MLK Drive

Cincinnati, Ohio 45268

513-569-7090 (office)

513-431-1970 (EPA mobile)

727-692-5333 (Personal mobile)

conmy.robyn@epa.gov

--

Dr. Michael H. Fulton-Estuaries and Land Use Branch Chief

Center for Coastal Environmental Health and

Biomolecular Research (CCEHBR)

USDOC/NOAA/NOS/NCCOS

219 Fort Johnson Road

Charleston, SC 29412-9110

voice: (843) 762-8576 fax: (843) 762-8700

e-mail: mike.fulton@noaa.gov

--

Dr. Michael H. Fulton-Estuaries and Land Use Branch Chief

Center for Coastal Environmental Health and

Biomolecular Research (CCEHBR)

USDOC/NOAA/NOS/NCCOS

219 Fort Johnson Road

Charleston, SC 29412-9110

voice: (843) 762-8576 fax: (843) 762-8700

e-mail: mike.fulton@noaa.gov

--

Dr. Michael H. Fulton-Estuaries and Land Use Branch Chief
Center for Coastal Environmental Health and
Biomolecular Research (CCEHBR)
USDOC/NOAA/NOS/NCCOS
219 Fort Johnson Road
Charleston, SC 29412-9110
voice: (843) 762-8576 fax: (843) 762-8700
e-mail: mike.fulton@noaa.gov

--

Dr. Michael H. Fulton-Estuaries and Land Use Branch Chief
Center for Coastal Environmental Health and
Biomolecular Research (CCEHBR)
USDOC/NOAA/NOS/NCCOS
219 Fort Johnson Road
Charleston, SC 29412-9110
voice: (843) 762-8576 fax: (843) 762-8700
e-mail: mike.fulton@noaa.gov

To: Conmy, Robyn[Conmy.Robyn@epa.gov]
Cc: Sundaravadivelu, Devi[sundaravadivelu.devi@epa.gov]; Grosser, Robert[Grosser.Robert@epa.gov]
From: Holder, Edith
Sent: Wed 6/8/2016 6:16:21 PM
Subject: RE: tomorrow

Robyn,

Yes, we are! We will be testing ANS against Dispersit SPC1000 and none. If things are running really smoothly, we could add the 2 method blanks for 35 ppt, one at 5 and the other at 25C. (There will be 20 method blanks scattered throughout the study, 2 at each salinity and temp combination to test glassware prep, etc.)

I will do the 5C testing concurrently while others do the 25C tests.

Also, I have 1L bottles muffled to ship to Hydrosphere along with the 2 dispersants -

Corexit 9500A and Finasol. Correct?

Anyhow, my understanding is that I can no longer just go into the file cabinet in 17? and pick up shipping labels. Is this correct? What is the current procedure and how much paperwork does it entail?

I want to send 2 coolers to Hydrosphere tomorrow.

Edie

From: Conmy, Robyn
Sent: Wednesday, June 08, 2016 1:37 PM
To: Holder, Edith <holder.edith@epa.gov>
Subject: tomorrow

Just checking that we are all set for tomorrow?

<>/<>/<>/<>/<>/<>/<>/<>/<>/<>/<>/<>/<>/<>/<>/<>/<>/<>

Robyn N. Conmy, Ph.D.

Research Ecologist

USEPA/NRMRL/LRPCD

26 West MLK Drive

Cincinnati, Ohio 45268

513-569-7090 (office)

513-431-1970 (EPA mobile)

727-692-5333 (Personal mobile)

conmy.robyn@epa.gov

To: Schubauer-Berigan, Joseph[Schubauer-Berigan.Joseph@epa.gov]
Cc: Conmy, Robyn[Conmy.Robyn@epa.gov]; McClellan, Kim[Mcclellan.Kim@epa.gov]; raghuraman.venkatapathy@ptsied.com[raghuraman.venkatapathy@ptsied.com]
From: Venkatapathy, Raghuraman
Sent: Wed 9/16/2015 8:54:48 PM
Subject: RE: Abstracts for 2016 GOMRI
ABSTRACT for Biodegradation of Finasol OSR 52 and Dispersed Alaska North Slope Crude Oil at 5 C and 25 C_SAJ.docx

Joe,

The revised abstract is attached.

Thanks,

raghu

Raghuraman Venkatapathy
On-Site Technical Manager
Pegasus Technical Services, Inc.
On-Site Contractor to U.S. EPA
NRMRL-STD/LRPCD, MS: 443
26 W. Martin Luther King Jr. Drive
Cincinnati, OH 45268.
Phone: (513) 569 7077 (O)/(513) 549 7880 (GV)
Fax: (513) 569 7677.
e-mail: venkatapathy.raghuraman@epa.gov

raghuraman.venkatapathy@ptsied.com

From: Schubauer-Berigan, Joseph
Sent: Wednesday, September 16, 2015 16:00
To: Venkatapathy, Raghuraman
Cc: Conmy, Robyn; McClellan, Kim; raghuraman.venkatapathy@ptsied.com
Subject: RE: Abstracts for 2016 GOMRI

We can clear the one that's been edited. The one I just sent needs to be addressed . thanks.

Joseph P. Schubauer-Berigan, Ph.D.

Chief, Environmental Stressors Management Branch
USEPA, Office of Research and Development
National Risk Management Research Laboratory
26 W. Martin Luther King Drive
Cincinnati, OH 45268
schubauer-berigan.joseph@epa.gov
Voice 513-569-7734
FAX 513-569-7620

From: Venkatapathy, Raghuraman
Sent: Wednesday, September 16, 2015 3:58 PM
To: Schubauer-Berigan, Joseph
Cc: Conmy, Robyn; McClellan, Kim; raghuraman.venkatapathy@ptsied.com
Subject: RE: Abstracts for 2016 GOMRI

Joe,

Yes, I can have her address the problems, and have them submitted today.

Thanks,

raghu

Raghuraman Venkatapathy
On-Site Technical Manager
Pegasus Technical Services, Inc.
On-Site Contractor to U.S. EPA
NRMRL-STD/LRPCD, MS: 443
26 W. Martin Luther King Jr. Drive
Cincinnati, OH 45268.
Phone: (513) 569 7077 (O)/(513) 549 7880 (GV)
Fax: (513) 569 7677.
e-mail: venkatapathy.raghuraman@epa.gov

raghuraman.venkatapathy@ptsied.com

From: Schubauer-Berigan, Joseph
Sent: Wednesday, September 16, 2015 15:57

To: Venkatapathy, Raghuraman
Cc: Conmy, Robyn; McClellan, Kim
Subject: RE: Abstracts for 2016 GOMRI

Ragu,

Still have a problem with the Yu Zhang abstract. See my comment in the attached abstract. I don't have her address. Can you please see that this is edited quickly. so we can move to clear it in STICS.

Thanks. Joe

Joseph P. Schubauer-Berigan, Ph.D.
Chief, Environmental Stressors Management Branch
USEPA, Office of Research and Development
National Risk Management Research Laboratory
26 W. Martin Luther King Drive
Cincinnati, OH 45268
schubauer-berigan.joseph@epa.gov
Voice 513-569-7734
FAX 513-569-7620

From: McClellan, Kim
Sent: Wednesday, September 16, 2015 3:28 PM
To: Venkatapathy, Raghuraman
Cc: Schubauer-Berigan, Joseph; Conmy, Robyn
Subject: Abstracts for 2016 GOMRI

Hi Raghu,

After the internal technical review was performed, two abstracts needed editorial changes. (see above in the attached files). Robyn Conmy's Branch Chief, Joe Schubauer-Berigan, approved the editorial changes for these two abstracts. I am making the changes to these two abstracts before I submit the abstracts to the clearance process.

Thanks,

Kim

To: Conmy, Robyn[Conmy.Robyn@epa.gov]; Sundaravadivelu, Devi[sundaravadivelu.devi@epa.gov]; Grosser, Robert[Grosser.Robert@epa.gov]
From: Holder, Edith
Sent: Fri 6/3/2016 8:07:05 PM
Subject: salinity bft expt

The test conditions for Monday are

35 ppt seawater

ANS oil

5C and 25C

Accell and Finasol OSR52

Edith L. Holder

Pegasus Technical Services, Inc.

On-Site Contractor to the U.S. EPA

ORD/NRMRL/LRPCD

26 W. Martin Luther King Dr.

Cincinnati, OH 45268

Phone: 513-569-7178

Email: holder.edith@epa.gov

To: Venkatapathy, Raghuraman[Venkatapathy.Raghuraman@epa.gov]
Cc: Conmy, Robyn[Conmy.Robyn@epa.gov]; McClellan, Kim[Mcclellan.Kim@epa.gov]
From: Schubauer-Berigan, Joseph
Sent: Wed 9/16/2015 7:57:04 PM
Subject: RE: Abstracts for 2016 GOMRI
ABSTRACT for Biodegradation of Finasol OSR 52 and Dispersed Alaska North Slope Crude Oil at 5 C and 25 C_SAJ.docx

Ragu,

Still have a problem with the Yu Zhang abstract. See my comment in the attached abstract. I don't have her address. Can you please see that this is edited quickly. so we can move to clear it in STICS.

Thanks. Joe

Joseph P. Schubauer-Berigan, Ph.D.
Chief, Environmental Stressors Management Branch
USEPA, Office of Research and Development
National Risk Management Research Laboratory
26 W. Martin Luther King Drive
Cincinnati, OH 45268
schubauer-berigan.joseph@epa.gov
Voice 513-569-7734
FAX 513-569-7620

From: McClellan, Kim
Sent: Wednesday, September 16, 2015 3:28 PM
To: Venkatapathy, Raghuraman
Cc: Schubauer-Berigan, Joseph; Conmy, Robyn
Subject: Abstracts for 2016 GOMRI

Hi Raghu,

After the internal technical review was performed, two abstracts needed editorial changes. (see above in the attached files). Robyn Conmy's Branch Chief, Joe Schubauer-Berigan, approved

the editorial changes for these two abstracts. I am making the changes to these two abstracts before I submit the abstracts to the clearance process.

Thanks,

Kim